

METALLOPHTHALOCYANINE-BASED ELECTRODE FOR SODIUM-ION BATTERIES



Mr. Apinut Chongphanitkul

A Thesis Submitted in Partial Fulfillment of the Requirements  
for the Degree of Master of Science in Chemistry

Department of Chemistry

Faculty of Science

Chulalongkorn University

Academic Year 2019

Copyright of Chulalongkorn University

ข้อไฟฟ้าฐานเมทลโลแทโลไซยานินสำหรับโซเดียมไอออนแบตเตอรี่



วิทยานิพนธ์นี้เป็นส่วนหนึ่งของการศึกษาตามหลักสูตรปริญญาวิทยาศาสตรมหาบัณฑิต  
สาขาวิชาเคมี ภาควิชาเคมี  
คณะวิทยาศาสตร์ จุฬาลงกรณ์มหาวิทยาลัย  
ปีการศึกษา 2562  
ลิขสิทธิ์ของจุฬาลงกรณ์มหาวิทยาลัย

Thesis Title METALLOPHTHALOCYANINE-BASED ELECTRODE FOR  
SODIUM-ION BATTERIES  
By Mr. Apinut Chongphanitkul  
Field of Study Chemistry  
Thesis Advisor Professor PATCHANITA THAMYONGKIT, Dr.rer.nat.  
Thesis Co Advisor PRASIT PATTANANUWAT, Ph.D.

---

Accepted by the Faculty of Science, Chulalongkorn University in Partial  
Fulfillment of the Requirement for the Master of Science

..... Dean of the Faculty of Science  
(Professor POLKIT SANGVANICH, Ph.D.)

THESIS COMMITTEE

..... Chairman  
(Associate Professor VUDHICHAJ PARASUK, Ph.D.)

..... Thesis Advisor  
(Professor PATCHANITA THAMYONGKIT, Dr.rer.nat.)

..... Thesis Co-Advisor  
(PRASIT PATTANANUWAT, Ph.D.)

..... Examiner  
(Assistant Professor ROJRIT ROJANATHANES, Ph.D.)

..... Examiner  
(Assistant Professor NUMPON INSIN, Ph.D.)

..... External Examiner  
(Assistant Professor Vorrada Loryuenyong, Ph.D.)

อภิสิทธิ์ จงพาศิลกุล : ขั้วไฟฟ้าฐานเมทัลโลแทลโลไซยานินสำหรับโซเดียมไอออนแบตเตอรี่. ( METALLOPHTHALOCYANINE-BASED ELECTRODE FOR SODIUM-ION BATTERIES) อ.ที่  
 บริการหลัก : ศ. ดร.พัชณิดา ธรรมรงค์กิจ, อ.ที่ปรึกษาร่วม : อ. ดร.ประสิทธิ์ พัฒนะนุวัฒน์

ในงานวิจัยนี้ ขั้วไฟฟ้าฐานเมทัลโลแทลโลไซยานินได้ถูกประดิษฐ์ขึ้นพร้อมทั้งศึกษาสมบัติทางเคมีไฟฟ้าและสมรรถภาพการกักเก็บพลังงาน ขั้วไฟฟ้า 6 ชนิดที่เตรียมขึ้นมาจากกระจกเคลือบอินเดียมทินออกไซด์ (ITO) ที่ถูกเคลือบด้วยอนุภาคทลวดนาโนไทเทเนียมไดออกไซด์ (TNT) พอลิ-3,4-เอทิลีนไอออกซีไทโอฟีน (PEDOT) และรีดิวซ์กราฟีนออกไซด์ (rGO) เพื่อเพิ่มความสามารถในการนำไฟฟ้าให้กับขั้วไฟฟ้า และเพิ่มพื้นที่ผิวให้กับวัสดุฐานเมทัลโลไซยานิน มอนอเมอร์ของแทลโลไซยานินเป้าหมายมีหมู่อะมิโนอยู่โดยรอบ และโลหะอะตอมกลางโคบอลต์(II) หรือนิกเกิล(II) บนพื้นผิวของขั้วไฟฟ้าแต่ละชนิดมีฟิล์มของมอนอเมอร์ที่เคลือบอยู่โดยเทคนิคการขึ้นรูปแบบหยด และฟิล์มพอลิเมอร์ของมอนอเมอร์ต่าง ๆ ถูกสร้างขึ้นด้วยปฏิกิริยาพอลิเมอร์เซชันเชิงเคมีไฟฟ้า จากการศึกษาพื้นที่ผิวที่ว่องไวทางเคมีไฟฟ้าของขั้วไฟฟ้าที่ถูกดัดแปลงและไม่ถูกดัดแปลงโดยเมทัลโลแทลโลไซยานิน พบว่ากรรมมี PEDOT ช่วยให้พื้นที่ผิวที่ว่องไวทางเคมีไฟฟ้าของขั้วไฟฟ้าเพิ่มขึ้นอย่างมีนัยสำคัญ การศึกษาความจุไฟฟ้าจำเพาะเบื้องต้นโดยใช้วิธีไซคลิกโวลแทมเมทรีและกลแวนออสเตดิกชาร์ตดิสชาร์ต ชี้ให้เห็นว่าฟิล์มพอลิเมอร์ของเมทัลโลแทลโลไซยานินนั้นสามารถเพิ่มความจุไฟฟ้าจำเพาะให้กับขั้วไฟฟ้าได้มีประสิทธิภาพมากกว่ามอนอเมอร์ TNT เพิ่มความจุไฟฟ้าจำเพาะเมื่อใช้ร่วมกับพอลิเมอร์ของนิกเกิล(II)-แทลโลไซยานินมากกว่าการใช้ร่วมกับพอลิเมอร์ของโคบอลต์(II)-แทลโลไซยานิน นอกจากนี้ rGO ก็สามารถเพิ่มความจุไฟฟ้าจำเพาะให้กับขั้วไฟฟ้าได้อย่างมีนัยสำคัญ ด้วยเหตุนี้ ขั้วไฟฟ้าที่ให้ ความจุไฟฟ้าจำเพาะที่มากที่สุด คือ ขั้วไฟฟ้าของพอลิเมอร์ของนิกเกิล(II)-แทลโลไซยานิน/PEDOT-rGO/TNT/กระจกเคลือบ ITO การศึกษาเพิ่มเติมถึงประสิทธิภาพในการกักเก็บพลังงานของขั้วไฟฟ้านี้ในการเป็นส่วนประกอบของโซเดียมไอออนแบตเตอรี่แสดงให้เห็นว่าแบตเตอรี่ให้ความจุไฟฟ้าจำเพาะมากถึง 60.22 มิลลิแอมป์ชั่วโมงต่อกรัมที่กระแสไฟฟ้า (ซีเรท) ที่ 3.94 ไมโครแอมป์ โดยมีร้อยละในการเก็บรักษาที่ 79.86 หลังจากผ่านไป 125 รอบของการประจุและคายประจุไฟฟ้า

จุฬาลงกรณ์มหาวิทยาลัย  
 CHULALONGKORN UNIVERSITY

สาขาวิชา เคมี  
 ปีการศึกษา 2562

ลายมือชื่อนิสิต .....  
 ลายมือชื่อ อ.ที่ปรึกษาหลัก .....  
 ลายมือชื่อ อ.ที่ปรึกษาร่วม .....



# # 6072010823 : MAJOR CHEMISTRY

KEYWORD: Metallophthalocyanine, Titanium dioxide nanotube, PEDOT, rGO, Energy storage

Apinut Chongphanitkul : METALLOPHTHALOCYANINE-BASED ELECTRODE FOR SODIUM-ION BATTERIES. Advisor: Prof. PATCHANITA THAMYONGKIT, Dr. rer. nat. Co- advisor: PRASIT PATTANANUWAT, Ph.D.

In this study, metallophthalocyanine-modified electrodes were fabricated and investigated for their electrochemical properties and energy storage performance. Six kinds of electrodes were prepared from indium tin oxide-coated glass (ITO-coated glass) substrates coated with titanium dioxide nanotube (TNT), poly(3,4-ethylenedioxythiophene) (PEDOT) and reduced graphene oxide (rGO) to improve conductivity of the substrates and surface area for the phthalocyanine-based materials. Target phthalocyanine monomers possess amino groups and Co(II) or Ni(II) central metals. On surface of each electrodes, films of the monomers were coated by a drop-casting technique, while those of their polymers were formed by electropolymerization. According to study on electrochemically active surface area of metallophthalocyanine-modified and unmodified electrodes, the presence of PEDOT significantly increases the electrochemically active surface area of the electrodes. Preliminary determination of specific capacitance of the electrodes by means of cyclic voltammetry (CV) and galvanostatic charge discharge (GCD) indicates that the metallophthalocyanine polymer films can more efficiently increase the specific capacitance of the electrodes than the monomers. TNT gives greater specific capacitance enhancement when used with the Ni(II)-phthalocyanine polymer films than when used with the Co(II)-phthalocyanine ones. Moreover, rGO also significantly improves the specific capacitance of the electrodes. Therefore, the electrode that give the optimum specific capacitance is the Ni(II)-phthalocyanine polymer film coated on PEDOT-rGO/TNT/ITO-coated glass. Further study for the energy storage performance of this electrode as a component of a sodium-ion battery shows that the specific capacitance of up to  $60.22 \text{ mAh} \cdot \text{g}^{-1}$  was obtained at a C-rate of 3.94  $\mu\text{A}$  with retention percentage of 79.86% after 125 charge/discharge cycles.

Field of Study: Chemistry

Academic Year: 2019

Student's Signature .....

Advisor's Signature .....

Co-advisor's Signature .....

## ACKNOWLEDGEMENTS

Foremost, I would like to express my deep gratitude to my thesis advisor Prof. Dr. Patchanita Thamyongkit and my co-advisor Dr. Prasit Pattanuwat for the continuous support of my study and research, for their patience, excellent guidance, stimulation, immense knowledge and valuable advice. Their kind guidance helped me in all the time of studying, doing the research as well as writing this thesis. My thesis could not be successful without their suggestions.

Besides my advisor, I would like to thank all of my thesis committee: Assoc. Prof. Dr. Vudhichai Parasuk for serving as the chairman, Asst. Prof. Dr. Rojrit Rojanathanes and Asst. Prof. Dr. Numpon Insin for serving as examiner and Asst. Prof. Vorrada Loryuenyong for serving as an external examiner from Silpakorn University.

In addition, I gratefully acknowledge the financial support of my entire master's degree study from H.M. the King Bhumibhol Adulyadej's 72nd Birthday Anniversary Scholarship, Graduate School, Chulalongkorn University

Special thanks also go to Prof. Dr. Julia Kunze-Liebhäuser and Dr. Engelbert Portenkirchner for laboratory facilities for sodium-ion battery fabrication, and all of members in the PT research group for helpful discussions and all of the supports during these years.

จุฬาลงกรณ์มหาวิทยาลัย  
CHULALONGKORN UNIVERSITY

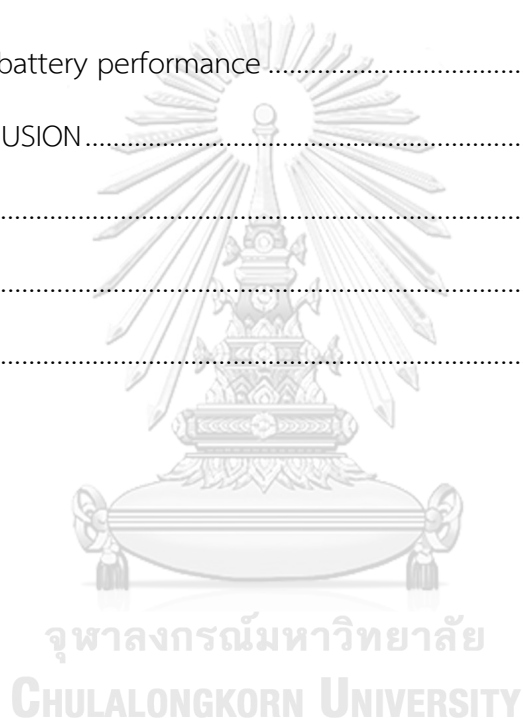
Apinut Chongphanitkul

## TABLE OF CONTENTS

	Page
ABSTRACT (THAI).....	iii
ABSTRACT (ENGLISH).....	iv
ACKNOWLEDGEMENTS .....	v
TABLE OF CONTENTS .....	vi
LIST OF FIGURES .....	ix
LIST OF SCHEMES .....	xii
LIST OF TABLES .....	xiii
CHAPTER I INTRODUCTION.....	1
1.1 Objectives of this research.....	3
1.2 Scopes of this research.....	3
CHAPTER II THEORY AND LITERATURE REVIEWS .....	4
2.1 Electrochemical analysis.....	4
2.1.1 Cyclic voltammetry (CV).....	4
2.1.2 Galvanostatic charge discharge (GCD) <sup>19</sup> .....	6
2.1.3 Galvanostatic cycling with potential limit (GCPL) .....	7
2.2 Materials.....	7
2.2.1 Phthalocyanine (Pc).....	7
2.2.2 Titanium dioxide nanotubes (TNT).....	13
2.2.3 Poly(3,4-ethylenedioxythiophene) (PEDOT) .....	14
2.2.4 Reduced graphene oxide (rGO).....	15
CHAPTER III EXPERIMENT .....	17

3.1 Synthesis .....	17
3.1.1 Materials and methods.....	17
3.1.2 Synthesis of 2,9,16,23-tetraaminophthalocyaninatocobalt(II) (Co-TAP) and 2,9,16,23-tetraaminophthalocyaninatonicel(II) (Ni-TAP) complexes.....	18
3.1.3 Preparation of titanium dioxide nanotube (TNT) .....	19
3.2 Electrode preparation .....	19
3.2.1 An ITO-coated glass (Electrode 1).....	19
3.2.2 A TNT film on the ITO-coated glass (TNT/ITO-coated glass, Electrode 2)	19
3.2.3 A PEDOT film on the ITO-coated glass (PEDOT/ITO-coated glass, Electrode 3).....	19
3.2.4 A PEDOT-rGO film on the ITO-coated glass (PEDOT-rGO/ITO-coated glass, Electrode 4).....	20
3.2.5 A PEDOT film on the TNT/ITO-coated glass (PEDOT/TNT/ITO-coated glass, Electrode 5) .....	20
3.2.6 A PEDOT-rGO film on the TNT/ITO-coated glass (PEDOT-rGO/TNT/ITO- coated glass, Electrode 6) .....	20
3.2.7 Phthalocyanine-modified electrodes.....	21
3.2.8 Electropolymerization of phthalocyanine monomers .....	21
3.3 Preliminary investigation on energy storage performance of the prepared electrodes .....	21
3.3.1 Determination of active surface area of the prepared electrodes by CV and Randles Sevcik equation.....	22
3.3.2 Investigation on specific capacitance of the prepared electrode by CV ..	22
3.3.3 Investigation on specific capacitance of the prepared electrode by GCD	23
3.3.4 Sodium-ion battery based on the phthalocyanine-based electrode .....	23
CHAPTER IV RESULTS AND DISCUSSION .....	25

4.1 Synthesis and characterization of the target phthalocyanines.....	25
4.2 Synthesis and characterization of TNT .....	27
4.3 Preparation of phthalocyanine-modified electrodes.....	27
4.3.1 Electrochemical deposition of PEDOT and PEDOT-rGO.....	28
4.3.2 Electropolymerization of phthalocyanine monomers .....	29
4.4 Preliminary studies on specific capacitance of the phthalocyanine-based electrodes .....	33
4.5 Sodium-ion battery performance .....	42
CHAPTER V CONCLUSION .....	46
APPENDIX.....	47
REFERENCES .....	57
VITA.....	65



## LIST OF FIGURES

Figure 1-1. Structure of the target molecules .....	2
Figure 1-2. Metallophthalocyanine based electrode series.....	3
Figure 2-1. A three-electrode one-compartment setup.....	4
Figure 2-2. (a) cyclic voltammetry potential waveform and (b) a cyclic voltammogram	5
Figure 2-3. (a) Ideal and (b) non-ideal galvanostatic charge discharge curves.....	6
Figure 2-4. A general structure of a metallophthalocyanine.....	8
Figure 2-5. a) polymerization of aniline and b) dimerization of aniline .....	8
Figure 2-6. Structures of (a) $4\beta$ -MTAPc and (b) $4\alpha$ -MTAPc (M = Co, Ni). .....	9
Figure 2-7. Cyclic voltammograms obtained from polymerization at GC electrode in DMF solution of 1 mM (a) $4\beta$ -NiTAPc and (b) $4\alpha$ -NiTAPc containing 0.1 M TBAP at a scan rate of $200 \text{ mV}\cdot\text{s}^{-1}$ . .....	9
Figure 2-8. AFM images obtained for (a) a bare ITO-coated glass and the polymerized films of (b) $4\beta$ -NiTAPc and (c) $4\alpha$ -NiTAPc on the ITO-coated glass electrodes .....	10
Figure 2-9. Cyclic voltammograms and DPV response of CoTnPc and $\text{SOCl}_2$ .....	11
Figure 2-10. (a) Cyclic voltammograms at various scan rates and (b) capacitance retention of CoPc/MWCNTs in 1 M $\text{H}_2\text{SO}_4$ .....	12
Figure 2-11. Cycle performance of phthalocyanines TN-NiPc (left) and TN- $\text{H}_2\text{Pc}$ (right) studied by Yeleng et al .....	12
Figure 2-12. Typical charge–discharge curves of an asymmetric supercapacitor based on $\text{RuO}_2/\text{TNT}$ at current densities of (a) 15, (b) 30, (c) 60 and (d) $120 \text{ mA}\cdot\text{cm}^{-2}$ .....	13
Figure 2-13. Typical charge-discharge curves of (a) $\text{V}_2\text{O}_5$ and (b) PEDOT/ $\text{V}_2\text{O}_5$ nanocomposites using a constant current density of $15 \text{ mA}\cdot\text{g}^{-1}$ studied by Murugan et al.	15

Figure 2-14. (a) Cyclic voltammograms at different scan rates and (b) GCD curves at different current densities of a PPy/rGO-based supercapacitor studied by Laua et al. ....	16
Figure 3-1. Electrochemical set up for active surface area calculation, CV and GCD..	22
Figure 3-2. Electrochemical setup for sodium-ion battery .....	23
Figure 3-3. a) Setup diagram of 'EL-CELL' and b) schematic cell stack.....	24
Figure 4-1. A TEM image of TNT .....	27
Figure 4-2. Cyclic voltammograms of all phthalocyanine-modified and unmodified electrodes .....	36
Figure 4-3. Cyclic voltammograms of a sodium-ion battery based on a poly(Ni-TAP)/ Electrode 6 at different scan rates in a potential range between 1.00 V and 3.00 V vs. Na/Na <sup>+</sup> .....	42
Figure 4-4. Galvanostatic charge/discharge curves of a sodium-ion battery at different C-rates between 1.00 V and 3.00 V vs. Na/Na <sup>+</sup> .....	43
Figure 4-5. Specific capacities of a sodium-ion battery at different C-rates at a potential range between 1.00 V and 3.00 V vs. Na/Na <sup>+</sup> .....	45
Figure S1. A MALDI-TOF Mass spectrum of Co-TAP .....	48
Figure S2. A MALDI-TOF Mass spectrum of Ni-TAP .....	48
Figure S3. An absorption spectrum of a Co-TAP solution in DMF .....	49
Figure S4. An absorption spectrum of a Ni-TAP solution in DMF .....	49
Figure S5. Images of the prepared electrode (a) without a phthalocyanine film, and with films of (b) Co-TAP (c) poly(Co-TAP) (d) Ni-TAP (e) poly(Ni-TAP) coated. ....	50

Figure S6. Cyclic voltammograms of phthalocyanine-modified and unmodified Electrode 1 in 1.0 M a KCl aqueous solution containing 5.0 mM $K_4Fe(CN)_6$ at scan rates of 5, 10, 30, 50, 100, 150 and 200 $mV \cdot s^{-1}$ .....	51
Figure S7. Cyclic voltammograms of phthalocyanine-modified and unmodified Electrode 2 in 1.0 M a KCl aqueous solution containing 5.0 mM $K_4Fe(CN)_6$ at scan rates of 5, 10, 30, 50, 100, 150 and 200 $mV \cdot s^{-1}$ .....	52
Figure S8. Cyclic voltammograms of phthalocyanine-modified and unmodified Electrode 3 in 1.0 M a KCl aqueous solution containing 5.0 mM $K_4Fe(CN)_6$ at scan rates of 5, 10, 30, 50, 100, 150 and 200 $mV \cdot s^{-1}$ .....	53
Figure S9. Cyclic voltammograms of phthalocyanine-modified and unmodified Electrode 4 in 1.0 M a KCl aqueous solution containing 5.0 mM $K_4Fe(CN)_6$ at scan rates of 5, 10, 30, 50, 100, 150 and 200 $mV \cdot s^{-1}$ .....	54
Figure S10. Cyclic voltammograms of phthalocyanine-modified and unmodified Electrode 5 in 1.0 M a KCl aqueous solution containing 5.0 mM $K_4Fe(CN)_6$ at scan rates of 5, 10, 30, 50, 100, 150 and 200 $mV \cdot s^{-1}$ .....	55
Figure S11. Cyclic voltammograms of phthalocyanine-modified and unmodified Electrode 6 in 1.0 M a KCl aqueous solution containing 5.0 mM $K_4Fe(CN)_6$ at scan rates of 5, 10, 30, 50, 100, 150 and 200 $mV \cdot s^{-1}$ .....	56



## LIST OF SCHEMES

Scheme 3-1. Synthesis procedure of target phthalocyanines.....	18
Scheme 4-1. Synthesis of tetraaminometallophthalocyanines .....	25
Scheme 4-2. Formation of tetranitrometallophthalocyanine .....	26



## LIST OF TABLES

Table 4-1. SEM images of Electrode 3 and Electrode 4 at 100, 1000 and 5000 magnification	29
Table 4-2. Cyclic voltammogram obtained from the electropolymerization of Co-TAP and Ni-TAP on Electrode 1 to Electrode 6	30
Table 4-3. Electrochemical active surface area of the unmodified and phthalocyanine-modified electrodes	35
Table 4-4. Specific capacitance of the unmodified and phthalocyanine-modified electrodes determined by CV method	37
Table 4-5. Specific capacitance of the unmodified and phthalocyanine-modified electrodes determined by a GCD method	39
Table 4-6. SEM images of unmodified Electrode 2 and unmodified and phthalocyanine-modified series of Electrode 6 at 100, 1000 and 5000 magnification	41

## CHAPTER I

### INTRODUCTION

In the 21st century, energy and environmental issues are globally recognized as major challenges that required efficient and sustainable approaches fitting people's daily lives without causing more pollution. As a key connection between various sources of alternative energy technology becomes a critical factor leading to an energy- and environmentally sustainable world as we desired, researchers have been trying to improve the overall performances of the existing energy storages. In terms of charging/discharging performance, safety, cost, sustainability and environmental friendliness.<sup>1,2,3</sup> The materials used in energy storage systems are conventionally metal-based inorganic compounds. However, production of the inorganic materials usually requires costly extraction and synthesis processes and generates harmful waste to the environment.<sup>4</sup> To overcome these problems, organic materials have been of great interest by offering possibilities to be produced through relatively inexpensive and scalable processes that can be easily modified and environmentally friendly.<sup>5</sup>

Among various organic compounds used as electrode components in many electrochemical applications, phthalocyanines constitute promising catalytic properties and offer advantages over metals and metal oxides because of their environmentally benign and lower cost.<sup>6,7</sup> Therefore, there are a wide variety of ways in which phthalocyanines (Pcs) and metallophthalocyanines (MPcs) have been employed in the energy storage system such as lithium/thionyl chloride batteries<sup>8</sup> lithium-air battery<sup>9</sup> and supercapacitor<sup>10</sup> etc. However, the organic materials do not exhibit high conductivity and need to be taken in conjunction with other conductive materials. Titanium dioxide nanotubes (TNT), poly(3,4-ethylene-dioxythiophene) (PEDOT) and reduced graphene oxide (rGO) have been widely used as the conductive materials in the energy storage applications. Some good examples include oriented NiO-TNT array

as electrodes in the supercapacitors,<sup>11</sup> directly grown amorphous TNT electrodes on current collectors in sodium-ion batteries,<sup>12</sup> PEDOT-coated rGO in a high-performance supercapacitor,<sup>13</sup> and PEDOT/MoS<sub>2</sub> nanocomposite for a small power rechargeable lithium battery.<sup>14</sup>

In this work, we are interested in synthesis and investigation of energy storage performance of the amino-substituted metallophthalocyanine derivatives, whose structures are shown in **Figure 1-1**, and of their polymer films on various kinds of substrates containing indium tin oxide (ITO)-coated glass, TNT, PEDOT and rGO substrate (**Electrode 1** to **Electrode 6**) as shown in **Figure 1-2**. Hypotheses of this work include (i) the peripheral amino groups on the phthalocyanine macrocycles will enable electropolymerization of the phthalocyanine monomers on the substrates, leading to the stable polymer films for using in the energy storage system; and (ii) the use of TNT which increase electrical conductivity and surface area, PEDOT which increase the electrical conductivity and  $\pi$ - $\pi$  interaction with the phthalocyanines and rGO which increase the surface area as the substrate materials will provide enhanced capacitive enhancement, compared with bare ITO-coated glass.

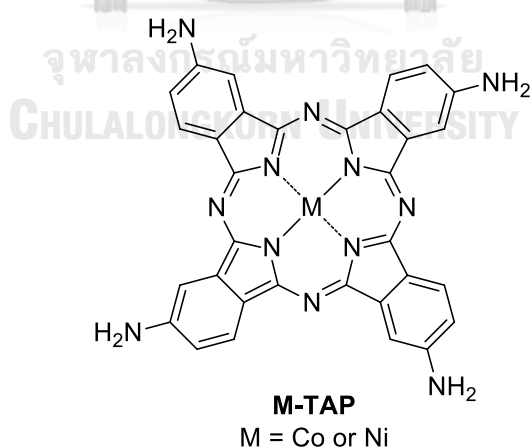


**Figure 1-1.** Structure of the target molecules

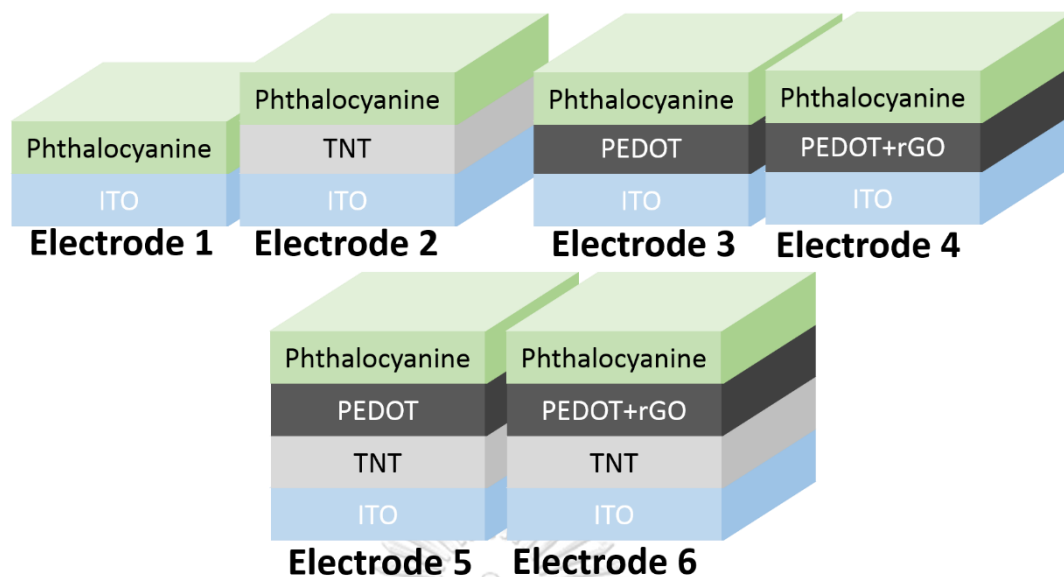


Figure 1-2. Metallophthalocyanine based electrode series

### 1.1 Objectives of this research

Synthesis and investigation of the photophysical properties and electrochemical properties, as well as the energy storage properties of the films of cobalt(II)- and nickel(II)-tetraaminophthalocyanines and of their polymers on various formulation of substrates including ITO-coated glass, TNT, PEDOT and rGO.

### 1.2 Scopes of this research

Each target tetraaminophthalocyanine monomer contained either cobalt(II) or nickel(II) as a central metal and were characterized by spectroscopic techniques, including mass spectrometry (MS) and UV-visible absorption spectrophotometry. TNT was synthesized and coated on the ITO-coated glass by a doctor blade method. PEDOT and rGO were electrochemically deposited on the substrates by chronopotentiometry. Electrochemical polymerization of the target monomers on the substrates was performed by cyclic voltammetry (CV). The resulting substrates were tested as working electrodes for their energy storage performance by CV and galvanostatic charge discharge (GCD).

## CHAPTER II

### THEORY AND LITERATURE REVIEWS

#### 2.1 Electrochemical analysis

##### 2.1.1 Cyclic voltammetry (CV)

The CV is a powerful electrochemical technique commonly employed to investigate the reduction and oxidation processes of molecular species. CV is also invaluable to study electron transfer-initiated chemical reactions.<sup>15</sup> Equipment required to perform CV is composed of a conventional potentiostat connected to three electrodes consisting of working (WE), reference (RE) and counter (CE) electrodes immersed in a supporting electrolyte as shown in **Figure 2-1**.<sup>16</sup>

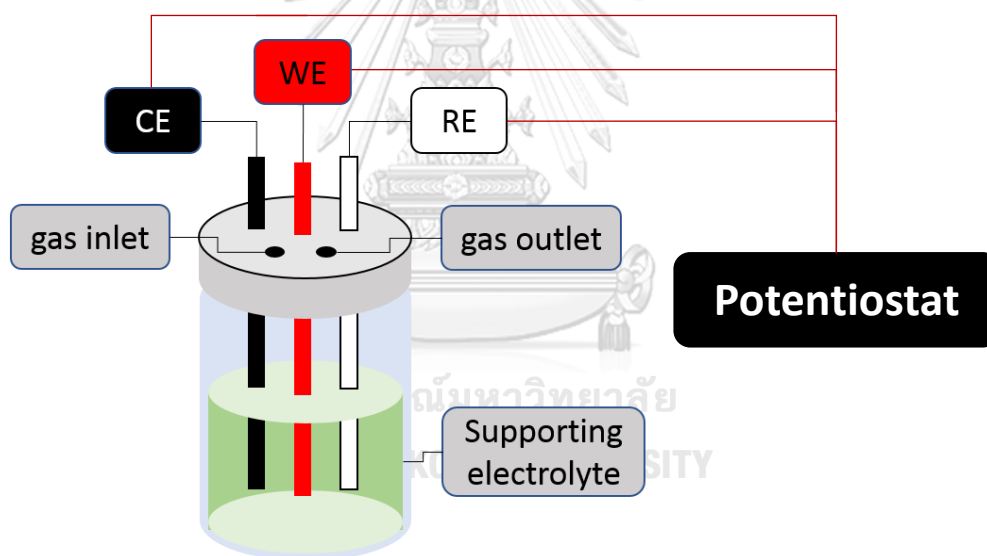


**Figure 2-1.** A three-electrode one-compartment setup

In the CV, electrode potential ramps linearly versus time in cyclical phases, as shown in **Figure 2-2a**. Rate of voltage change over time during each of these phases is known as the scan rate ( $V \cdot s^{-1}$ ). The potential is measured between the WE and the RE, while the current is measured between the WE and the CE. These data are plotted as current versus applied potential to give a cyclic voltammogram as shown in **Figure 2-2b**.

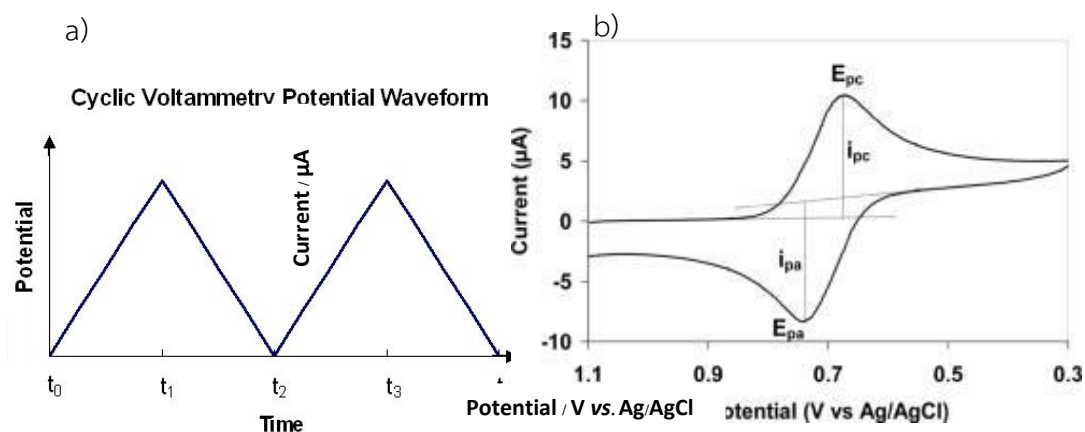


Figure 2-2. (a) cyclic voltammetry potential waveform and (b) a cyclic voltammogram

In the cyclic voltammogram, a forward scan yields anodic current for every analyte that can be oxidized in the range of the scanned potential. In the opposite direction, a reverse scan produces cathodic current for products of the forward scan being reduced. Thus, there are reduction and oxidation peaks observed for a reversible redox reaction. Significant parameters in the cyclic voltammogram are cathodic peak potential ( $E_{pc}$ ), anodic peak potential ( $E_{pa}$ ), cathodic peak current ( $i_{pc}$ ) and anodic peak current ( $i_{pa}$ ), describing electrochemical behavior of each substance.<sup>17</sup>

The CV is also a fundamental technique popularly used in energy storage studies. The cyclic voltammogram can not only represent electrochemical behavior, but also specific capacitance of the tested electrode. The specific capacitance can be calculated by equation (1).<sup>18</sup>

$$C_s = \frac{\int I(V)dV}{2\mu m \Delta V} \quad (1)$$

where  $C_s$  = specific capacitance ( $\text{F}\cdot\text{g}^{-1}$  or  $\text{F}\cdot\text{m}^{-2}$ )

$\int I(V)$  = integrated area under curve of cyclic voltammogram ( $\text{F}\cdot\text{V}^2\cdot\text{s}^{-1}$ )

$\mu$  = scan rate ( $\text{V}\cdot\text{s}^{-1}$ )

$m$  = mass or surface area of active material (g or  $\text{m}^2$ )

$\Delta V$  = potential range (V)

### 2.1.2 Galvanostatic charge discharge (GCD)<sup>19</sup>

The GCD is a standard technique used to test the performance of electrical double layer capacitors (EDLCs) and batteries. The tested energy storage is charged and discharged between two specified voltage points at a constant applied current. Generally, there are 2 types of the constant current *i.e.* positive constant current for a charging process and negative constant current for a discharging process. This technique can more accurately reflect real-world performance than the cyclic voltammetry. Ideally, the resulting plot of the voltage over the time is linear with alternating positive and negative slopes. Deviations from linearity may occur by series resistance causing the cell voltage to drop rapidly called IR drop, as shown in **Figure 2-3**.

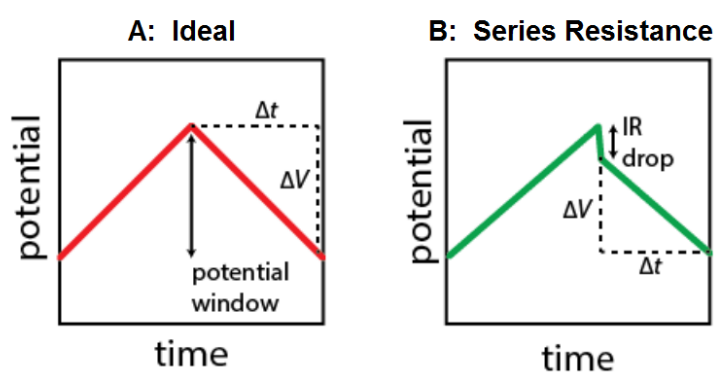


**Figure 2-3.** (a) Ideal and (b) non-ideal galvanostatic charge discharge curves

The GCD also can represent the specific capacitance of the tested cells.

The specific capacitance can be calculated by equation (2).<sup>18</sup>

$$C_s = \frac{I\Delta t}{m\Delta V} \quad (2)$$

where  $C_s$  = specific capacitance ( $F \cdot g^{-1}$  or  $F \cdot m^{-2}$ )

$I$  = applied constant discharge current ( $F \cdot V \cdot s^{-1}$ )

$\Delta t$  = discharging time (s)

$m$  = mass or surface area of active material (g or  $m^2$ )

$\Delta V$  = potential range (V)



### 2.1.3 Galvanostatic cycling with potential limit (GCPL)

Galvanostatic cycling with potential limit (GCPL) is similar to the GCD, but with a repetitive loop of the charging and discharging cycle. This protocol corresponds to the most standard for studying the behavior of batteries upon cycling. The performance of the batteries is determined as a function of its charge and discharge conditions. When studying an electrode, the specific capacity of the electrode is often considered as milliampere hour per active material weight ( $\text{mAh}\cdot\text{g}^{-1}$ ).<sup>20</sup> Charge and discharge rates are often given as C or C-rate, which is a measure of the rate at which a battery is charged or discharged relative to its capacity. The unit of the C-rate is  $\text{h}^{-1}$ , equivalent to stating the battery's capacity to store an electrical charge in unit hour times current in the same unit as the charge or discharge current. For example, for a battery with a capacity of 500 mAh, a discharge rate of 250 mA corresponds to a C-rate of 1/2 (C/2), meaning that this current can discharge half of this batteries in one hour.<sup>21</sup>

## 2.2 Materials

### 2.2.1 Phthalocyanine (Pc)

Pc is a large, aromatic, macrocycle, organic compound with the chemical formula of  $(\text{C}_8\text{H}_4\text{N}_2)_4\text{H}_2$ , whose structure is shown in **Figure 2-4**.<sup>22</sup> It is composed of four isoindole units linked by nitrogen atoms. Pc has many remarkable properties such as high stability, remarkable photophysical properties and good redox reversibility, and offer various possibilities for structural modification.<sup>23,24,25</sup> The electrochemical and photophysical properties can be modified by adding the central metal atom or substituents on the macrocycle peripheral. In addition, Pc that has 4 substituents on the Pc is having more stability and better solubility than that with more substituents.<sup>26,27,28</sup>

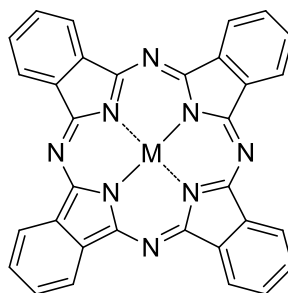


**Figure 2-4.** A general structure of a metallophthalocyanine

In the presence of an electrochemically polymerizable group, such as an aniline unit, Pc can be polymerized by applying the appropriate potential to induce the polymerization on the aniline units. Anodic oxidation of the amino groups on the aniline units can lead to polymer formation on the surface of the working electrode.<sup>29,30</sup> There are generally two mechanisms proposed for the electrochemical polymerization of aniline, as shown in **Figure 2-5**.

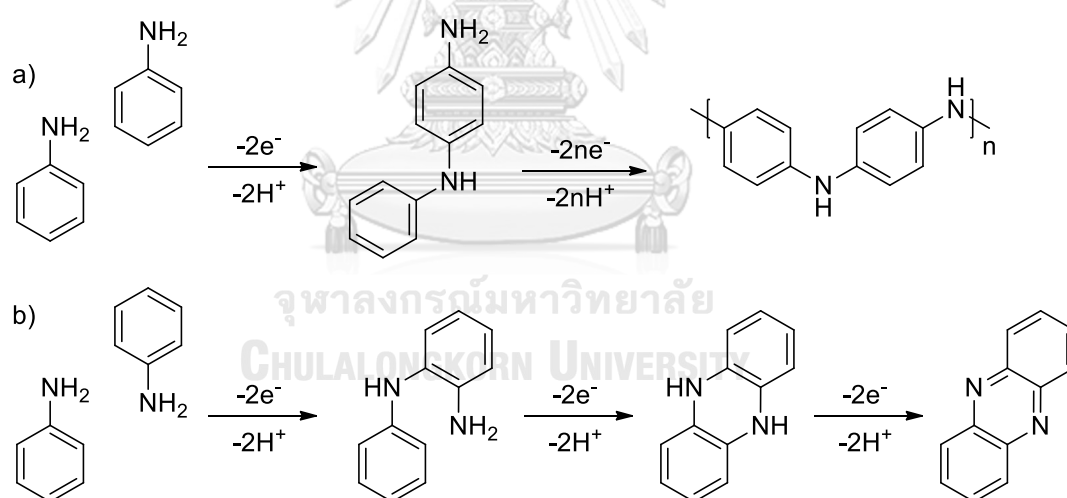


**Figure 2-5.** a) polymerization of aniline and b) dimerization of aniline<sup>29</sup>

In 2008, Sivanesan and Abraham<sup>31</sup> electropolymerized tetraaminometallophthalocyanines (MTAPcs; M = Ni and Co) having amino groups at  $\alpha$ - ( $4\alpha$ -MTAPc, **Figure 2-6a**) and  $\beta$ - ( $4\beta$ -MTAPc, **Figure 2-6b**) positions on glassy carbon and ITO electrodes. As shown in **Figure 2-7**, they successfully electropolymerized these compounds by means of CV in the three-electrode system in a potential range

between  $-0.15$  to  $0.90$  V vs. Ag/AgCl in dimethylformamide (DMF) containing  $1$  mM  $4\alpha$ -MTAPc or  $4\beta$ -MTAPc and  $0.1$  M tetrabutylammonium perchlorate (TBAP) at the scan rate of  $200$   $\text{mV}\cdot\text{s}^{-1}$  for 30 cycles. Furthermore, the results also showed that the electropolymerization growth rate of  $4\alpha$ -MTAPc was less than that of  $4\beta$ -MTAPc prepared under the same condition. Moreover, the surface coverage of the  $4\beta$ -MTAPc film was greater than that of the  $4\alpha$ -MTAPc film according to atomic force microscope (AFM) images (Figure 2-8).

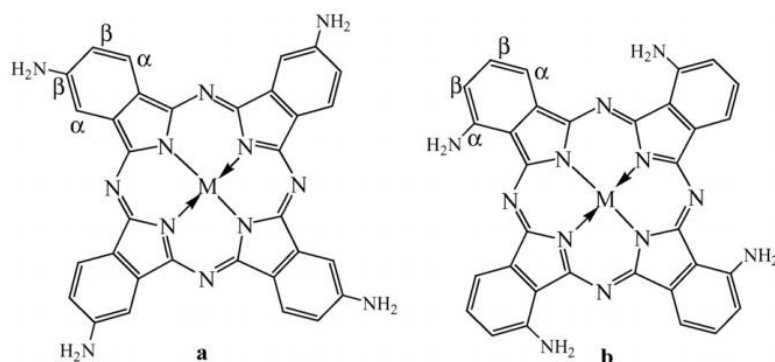


Figure 2-6. Structures of (a)  $4\beta$ -MTAPc and (b)  $4\alpha$ -MTAPc ( $M = \text{Co}, \text{Ni}$ ).<sup>31</sup>

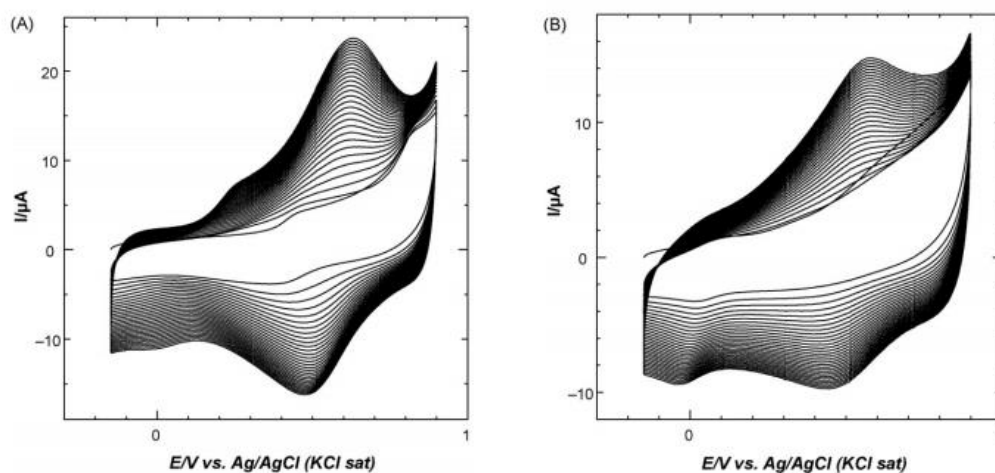
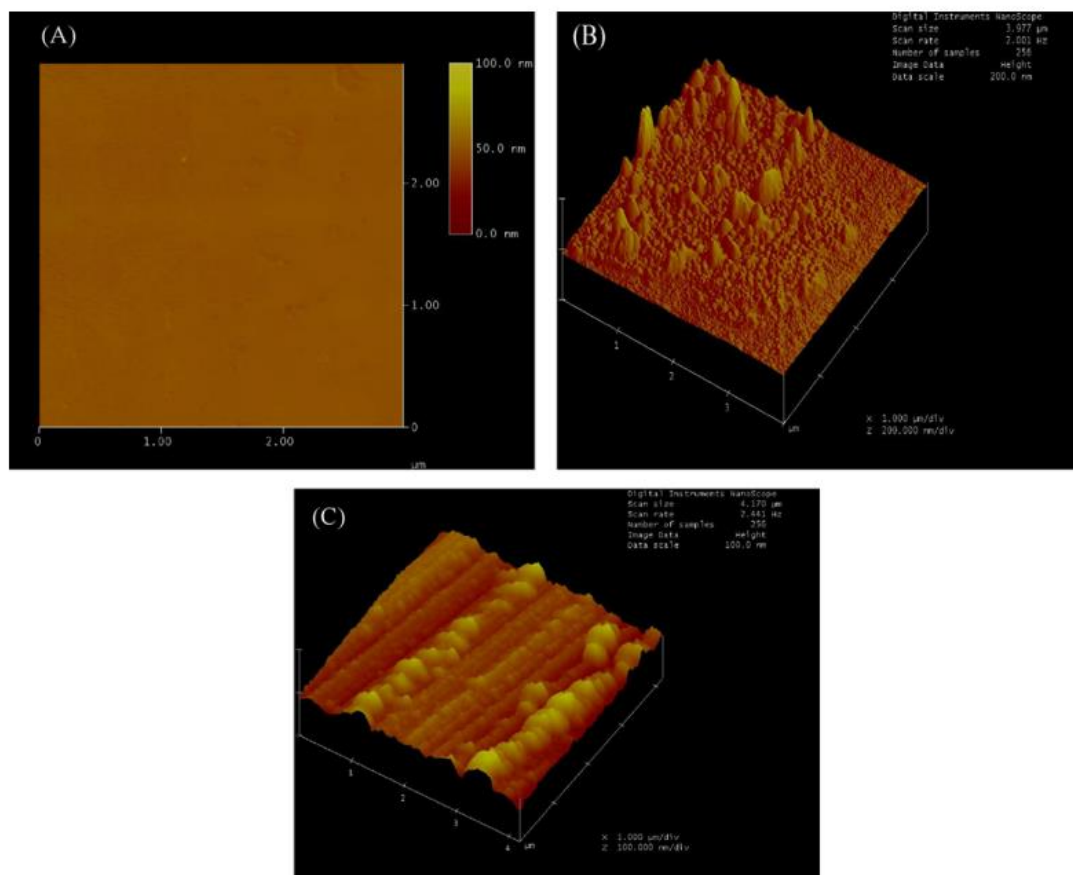
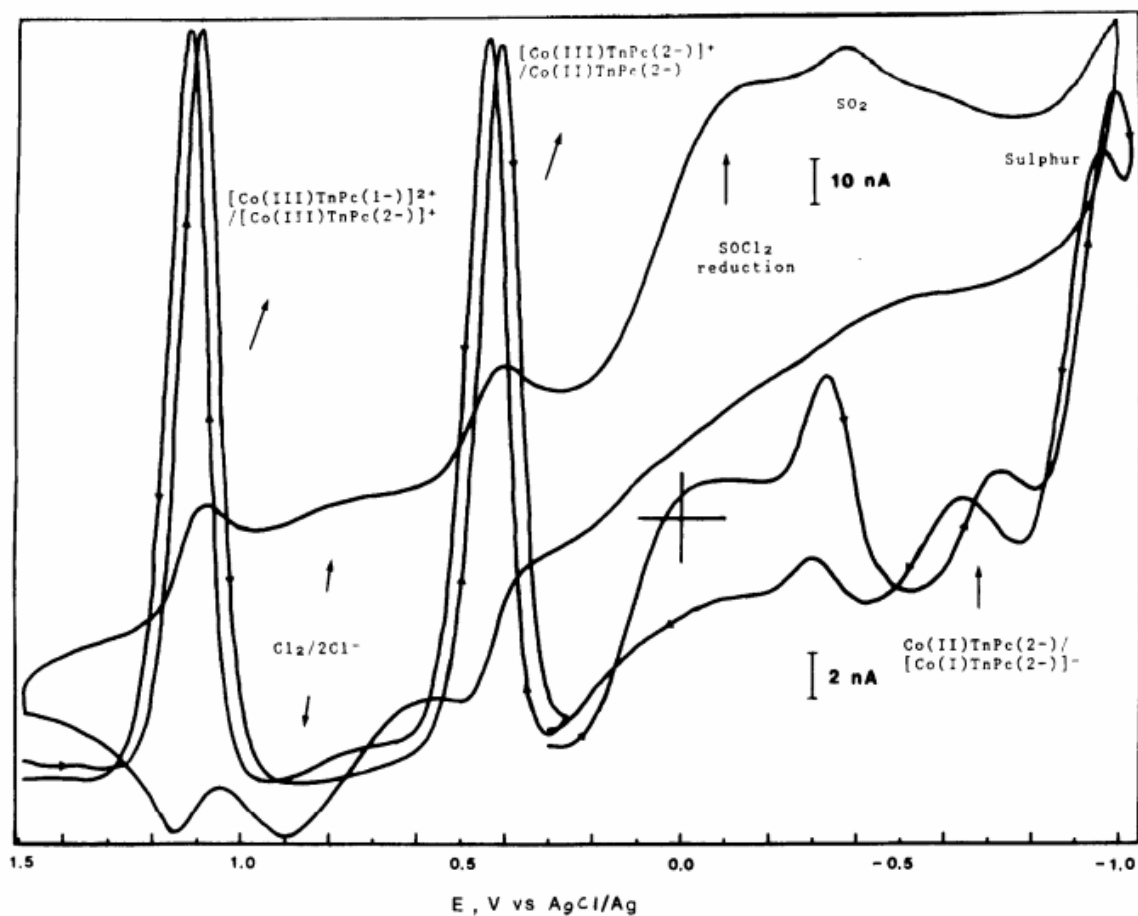


Figure 2-7. Cyclic voltammograms obtained from polymerization at GC electrode in DMF solution of  $1$  mM (a)  $4\beta$ -NiTAPc and (b)  $4\alpha$ -NiTAPc containing  $0.1$  M TBAP at a scan rate of  $200$   $\text{mV}\cdot\text{s}^{-1}$ .



**Figure 2-8.** AFM images obtained for (a) a bare ITO-coated glass and the polymerized films of (b)  $4\beta$ -NiTAPc and (c)  $4\alpha$ -NiTAPc on the ITO-coated glass electrodes

As for the field of energy storage, MPcs has been involved in many electrochemical energy storage researches for ages. In 1989, Bernstein and Lever<sup>32</sup> studied by the CV, differential pulse voltammetry (DPV) and electronic spectroscopy a reaction between thionyl chloride ( $\text{SOCl}_2$ ) and a cobalt phthalocyanine derivative in a lithium/ thionyl chloride battery. The results showed that  $\text{SOCl}_2$  reacted with  $[\text{Co}^{1+}\text{TnPc}]^-$  and  $\text{CoTnPc}$  to give two-electron-oxidized species as shown in **Figure 2-9**, indicating as a key reduction process of  $\text{SOCl}_2$  in this kind of battery.



**Figure 2-9.** Cyclic voltammograms and DPV response of CoTnPc and  $\text{SOCl}_2$

In 2012, Zhanwei et al.<sup>33</sup> prepared cobalt phthalocyanine molecules composited with multiwalled carbon nanotubes (CoPc/MWCNTs) by microwave-assisted process. This CoPc/MWCNTs was used as the electrode for an electrochemical capacitor that operated at the very high scan rates. As shown in **Figure 2-10a**, the cyclic voltammograms at the scan rate of  $500 \text{ mV}\cdot\text{s}^{-1}$  showed an almost perfect rectangular shape, indicating good electrical conductivity. Moreover, the supercapacitor was stable in  $1 \text{ M H}_2\text{SO}_4$  with capacitance retention percentage of 98% after 10,000 cycles as shown in **Figure 2-10b**.

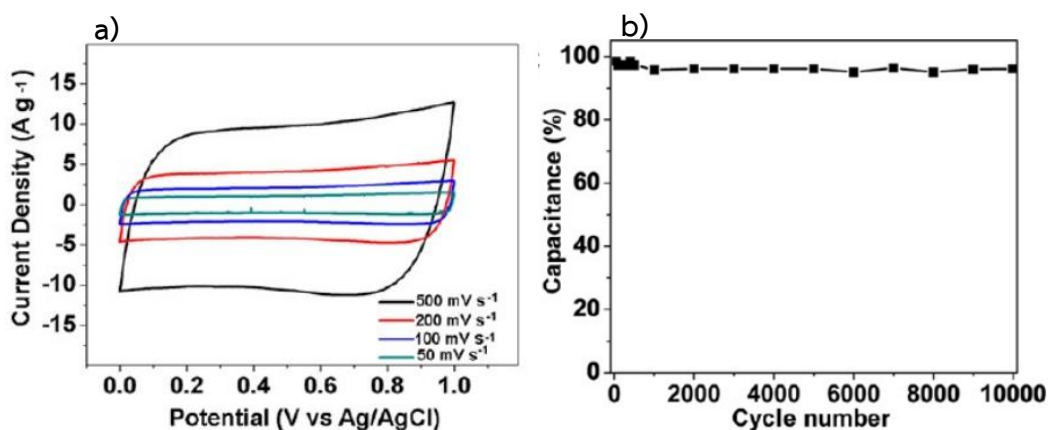


Figure 2-10. (a) Cyclic voltammograms at various scan rates and (b) capacitance retention of CoPc/MWCNTs in 1 M H<sub>2</sub>SO<sub>4</sub><sup>33</sup>

In 2017, Yekang et al<sup>34</sup> synthesized Tetra- $\beta$ -nitro-substituted nickel(II) phthalocyanine (TN-NiPc) and hollow phthalocyanine (TN-H<sub>2</sub>Pc). When the two H atoms in the center of TN-H<sub>2</sub>Pc were substituted with the Ni atoms, interactive force between the phthalocyanine rings was lessened, resulted in a fluffy morphology for TN-NiPc that was beneficial to the insertion of lithium ions. Therefore, better electrochemical properties and reversibility were observed in the TN-NiPc electrode compared to the TN-H<sub>2</sub>Pc one. The capacity of the TN-NiPc electrode was stable at about 280 mAh $\cdot$ g<sup>-1</sup> at 0.2 C after 250 cycles at several different current rates of 0.1, 0.2, 0.5, and 1 C as shown in Figure 2-11.

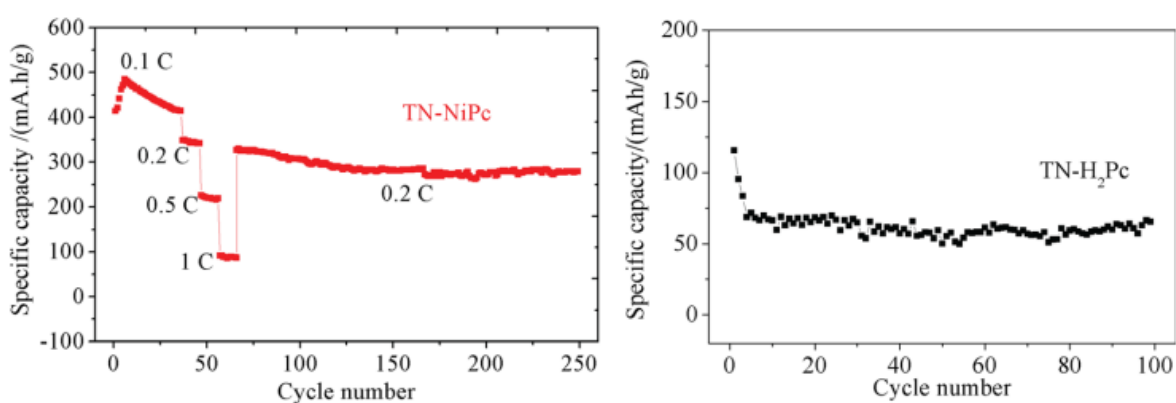
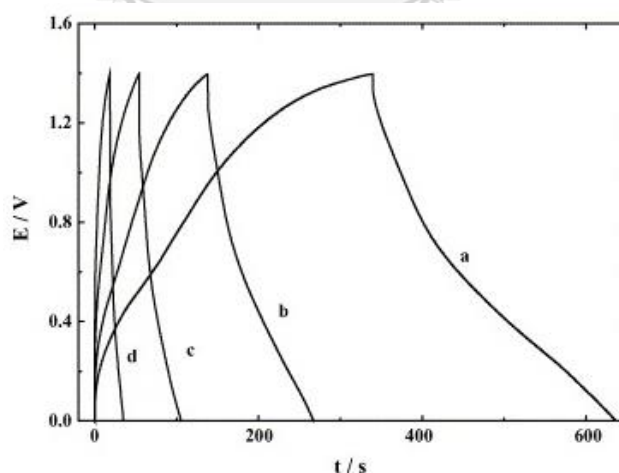


Figure 2-11. Cycle performance of phthalocyanines TN-NiPc (left) and TN-H<sub>2</sub>Pc (right) studied by Yeleng et al<sup>34</sup>

### 2.2.2 Titanium dioxide nanotubes (TNT)

TiO<sub>2</sub>, also known as titanium(IV) oxide or titania, is naturally occurring oxide of titanium. TiO<sub>2</sub> can be produced in particle size of nanometers having photocatalytic properties and is environmentally friendly. With these properties, wide fields of applications has brought the TiO<sub>2</sub> nanoparticles to be a popular material.<sup>35,36</sup> Moreover, the morphology of the TiO<sub>2</sub> nanoparticles can be developed into various shapes including nanotubes that exhibit outstanding surface area and better photocatalytic properties than the TiO<sub>2</sub> nanoparticles.<sup>37,38</sup> The data from these researches is very useful for the development of the energy storage systems because one way to improve the system performance is to increase the surface area of the electrode.<sup>39</sup> Yong-Gang et al<sup>40</sup> developed an asymmetric supercapacitor where a RuO<sub>2</sub>/TNT composite was used as the positive electrode and the activated carbon as the negative electrode in a 1 mol/L KOH electrolyte solution. A power density of 1207 W•kg<sup>-1</sup> was obtained with energy density of 5.7 W•h•kg<sup>-1</sup> and the charge–discharge current density of 120 mA•cm<sup>-2</sup> as shown in **Figure 2-12**.



**Figure 2-12.** Typical charge–discharge curves of an asymmetric supercapacitor based on RuO<sub>2</sub>/TNT at current densities of (a) 15, (b) 30, (c) 60 and (d) 120 mA•cm<sup>-2</sup>





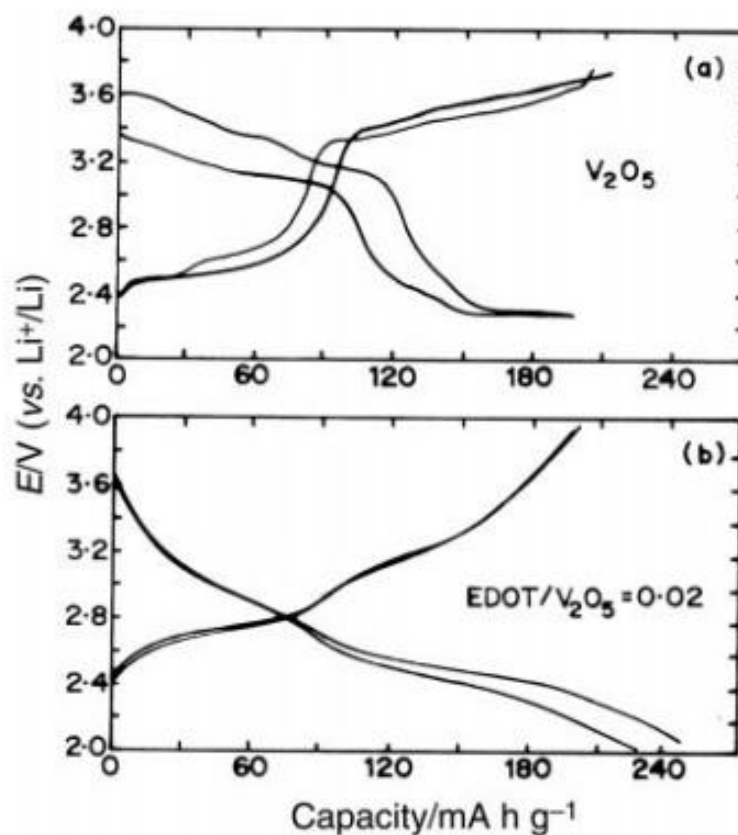
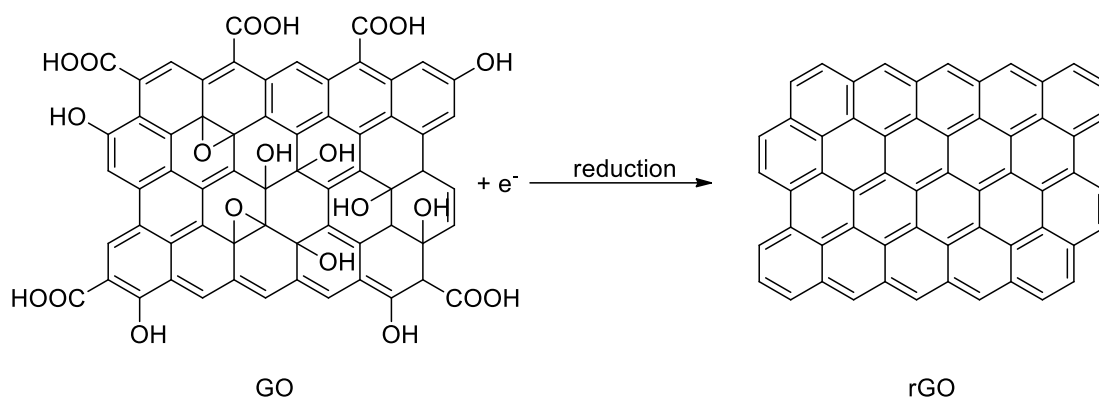


**Figure 2-13.** Typical charge-discharge curves of (a)  $V_2O_5$  and (b) PEDOT/ $V_2O_5$  nanocomposites using a constant current density of  $15 \text{ mA}\cdot\text{g}^{-1}$  studied by Murugan et al.<sup>45</sup>

#### 2.2.4 Reduced graphene oxide (rGO)

Graphene, a two-dimensional nanostructure of carbon, has attracted a great deal of attention due to its special monolayer structure resulting in many favorable properties, such as good chemical stability and extraordinary electronic transport properties.<sup>46</sup> Graphene oxide (GO) has been widely used as a starting material for synthesis of processible graphene.<sup>47</sup> GO is most commonly reduced by chemical and thermal treatments in order to remove the oxygen-containing functional groups.<sup>48</sup> In this research, we are using the free electrons that released from the formation of EDOT radical cations and causes *in-situ* reduction of GO into rGO as shown in **Scheme 2-2**.<sup>49</sup>



**Scheme 2-2.** Reduction of GO

rGO also has been widely utilized in the energy storage applications. Laua et al.<sup>50</sup> developed a symmetrical supercapacitor based on polypyrrole/rGO (PPy/rGO) and integrated it with a dye-sensitized solar cell. This PPy/rGO-based supercapacitor gave the large peak area under the cyclic voltammogram, indicating good capacitance as shown in **Figure 2-14a** and showed high calculated specific capacitances with values of 308.1, 277.6, 227.2, 222.5, and 225.1  $\text{F}\cdot\text{g}^{-1}$  at the current densities of 1, 2, 3, 4, and 5  $\text{A}\cdot\text{g}^{-1}$ , respectively as shown in **Figure 2-14b**.

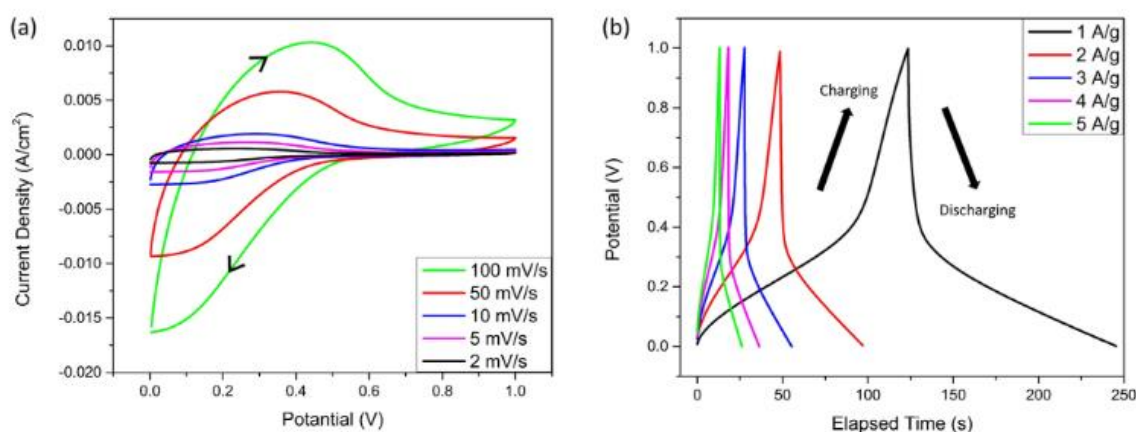


**Figure 2-14.** (a) Cyclic voltammograms at different scan rates and (b) GCD curves at different current densities of a PPy/rGO-based supercapacitor studied by Laua et al.<sup>50</sup>

## CHAPTER III

### EXPERIMENT

#### 3.1 Synthesis

##### 3.1.1 Materials and methods

All chemicals used in this work were purchased from commercial sources and used as received without further purification, unless noted otherwise.

Mass spectra were obtained using matrix-assisted laser desorption ionization time-of-flight mass spectrometry (MALDI-TOF-MS) with  $\alpha$ -cyano-4-hydroxy cinnamic acid ( $\alpha$ -CCA) as a matrix.

Absorption spectra of solution in dimethyl formamide (DMF) and films on the ITO-coated glass of the target phthalocyanine were recorded by an Agilent Cary 60 ultraviolet-visible spectrophotometer at room temperature.

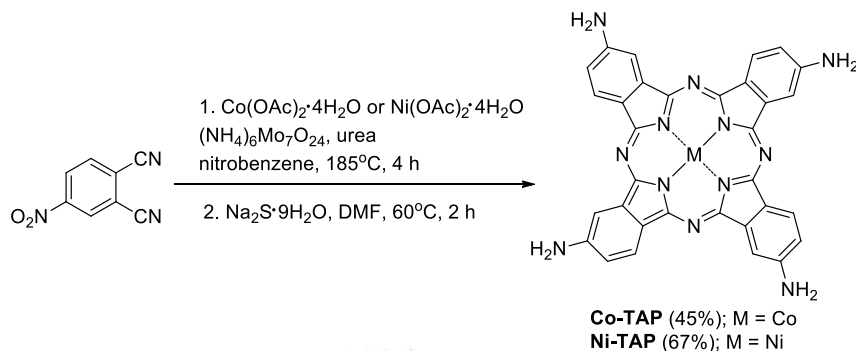
TiO<sub>2</sub> nanotubes morphology were characterized by a Philips TECNAI 20 transmission electron microscope (TEM).

Surface morphology of the prepared electrodes were investigated by a JEOL JSM-IT100 scanning electron microscope (SEM) at 100 1000 and 5000 magnification.

Electrochemical deposition process, electropolymerization of the phthalocyanine monomers and preliminary study of prepared electrode were performed using a Metrohm-Autolab PGSTAT101 potentiostat.

Investigation of sodium-ion battery performance by the CV and GCPL were performed by using a BioLogic VMP3 system with an EC-Lab software and a 'EL-CELL electrochemical setup.

### 3.1.2 Synthesis of 2,9,16,23-tetraaminophthalocyaninatocobalt(II) (Co-TAP) and 2,9,16,23-tetraaminophthalocyaninatonicel(II) (Ni-TAP) complexes



**Scheme 3-1.** Synthesis procedure of the target phthalocyanines

Following a published procedure,<sup>51</sup> a solution of 4-nitrophthalonitrile (0.870 g, 5.03 mmol),  $\text{Co}(\text{OAc})_2 \cdot 4\text{H}_2\text{O}$  (0.375 g, 1.51 mmol) or  $\text{Ni}(\text{OAc})_2 \cdot 4\text{H}_2\text{O}$  (0.368 g, 1.51 mmol),  $(\text{NH}_4)_6\text{Mo}_7\text{O}_{24} \cdot 4\text{H}_2\text{O}$  (0.013 g, 0.066 mmol) and urea (1.550 g, 25.83 mmol) in nitrobenzene (15.0 mL) was heated at  $185^\circ\text{C}$  for 4 h. After the reaction mixture was cooled to room temperature, the resulting precipitate was filtered off and washed with methanol:diethyl ether (1:9) and water. After that, following a known procedure,<sup>52</sup> the precipitate was dissolved in DMF and reacted with  $\text{Na}_2\text{S} \cdot 9\text{H}_2\text{O}$  under  $\text{N}_2$  atmosphere at  $60^\circ\text{C}$  for 2 h. Then, the solution mixture was diluted with water (15.0 mL) and the pH was adjusted to 7 by adding concentrated HCl. Subsequently, the precipitate was collected by filtration and washed with methanol:diethyl ether (1:9) and then water to obtain **Co-TAP** (0.361 g, 45%) or **Ni-TAP** (0.537, 67%) as a dark green solid.

**Co-TAP** : MALDI-TOF-MS obsd 631.227 ( $[\text{M}^+]$ ), calcd 631.127

( $[\text{M}^+]$ , M =  $\text{C}_{32}\text{H}_{20}\text{N}_{12}\text{Co}$ ) (**Figure S1**);  $\lambda_{\text{obs}}$  322, 411, 647, 719 nm. (**Figure S3**)

**Ni-TAP** : MALDI-TOF-MS obsd 630.174 ( $[\text{M}^+]$ ), calcd 631.129

( $[\text{M}^+]$ , M =  $\text{C}_{32}\text{H}_{20}\text{N}_{12}\text{Ni}$ ) (**Figure S2**);  $\lambda_{\text{obs}}$  311, 427, 648, 721 nm. (**Figure S4**)

### 3.1.3 Preparation of titanium dioxide nanotube (TNT)

Following a known procedure,<sup>53</sup> TiO<sub>2</sub> anatase powder (1.019 g) in a 10 M NaOH aqueous solution (30.0 mL) in a Teflon cup was heated in an autoclave at hydrothermal temperature of 135 °C for 24 h. After the reaction mixture was cooled to room temperature, the resulting precipitate was filtered off and adjusted the pH to 7 by adding a 1.0 M HCl aqueous solution to obtain TNT (0.927 g, 91%) as white solid. The TNT was characterized by the TEM afterwards.

## 3.2 Electrode preparation

### 3.2.1 An ITO-coated glass (Electrode 1)

An ITO-coated glass was cleaned by sonication in 2-propanol, acetone and milli-Q water for 15 min each and then leaving to dry under ambient condition before use to obtain **Electrode 1**.

### 3.2.2 A TNT film on the ITO-coated glass (TNT/ITO-coated glass, Electrode 2)

Following a standard procedure,<sup>54</sup> the TNT obtained from section 3.1.3 (0.030 g) was mixed with milli-Q water:acetic acid (3:1, 2.0 mL) and then dispersed by sonication for 30 min. The resulting TNT paste was spread on 1 cm x 2 cm area of **Electrode 1** that was framed by a layer of 3M adhesive tape (63 μm thick) by a doctor blade technique. After that, the resulted electrode was sintered at 400 °C for 1 h in air to obtain **Electrode 2**.

### 3.2.3 A PEDOT film on the ITO-coated glass (PEDOT/ITO-coated glass, Electrode 3)

Electrochemical deposition of the PEDOT film on the **Electrode 1** was performed in a three- electrode one-compartment electrochemical cell consisting of **Electrode 1** as the WE, a platinum plate as the CE and silver chloride-coated on a silver wire (Ag/AgCl) quasi-reference electrode (QRE). A 0.1 M H<sub>2</sub>SO<sub>4</sub> aqueous solution was used as a supporting electrolyte and contained 0.01 M EDOT.

The electropolymerization of EDOT was carried out at a constant potential of 0.90 V vs. Ag/AgCl QRE for 5 min.<sup>55,56</sup> Then, the WE was removed from the solution and rinsed with milli-Q water, resulting in **Electrode 3** having a dark blue film of PEDOT.

#### 3.2.4 A PEDOT-rGO film on the ITO-coated glass (PEDOT-rGO/ITO-coated glass, Electrode 4)

In a similar electrochemical setup as that described for the preparation of **Electrode 3**, except that a 0.1 M H<sub>2</sub>SO<sub>4</sub> aqueous solution containing 0.01 M EDOT and 1.0 mg/mL GO was used as the supporting electrolyte. **Electrode 4** was obtained after the rinsing step with a dark blue film of PEDOT-rGO observed.

#### 3.2.5 A PEDOT film on the TNT/ITO-coated glass (PEDOT/TNT/ITO-coated glass, Electrode 5)

In a similar electrochemical setup as that described for the preparation of **Electrode 3**, except that **Electrode 2** was used as the WE, **Electrode 5** was obtained after the rinsing step with a dark blue film of PEDOT observed.

#### 3.2.6 A PEDOT-rGO film on the TNT/ITO-coated glass (PEDOT-rGO/TNT/ITO-coated glass, Electrode 6)

In a similar electrochemical setup as that described for the preparation of **Electrode 3**, except that **Electrode 2** was used as the WE and 0.1 M H<sub>2</sub>SO<sub>4</sub> aqueous solution containing 0.01 M EDOT and 1.0 mg/mL GO was used as the supporting electrolyte. **Electrode 4** was obtained after the rinsing step with a dark blue film of PEDOT-rGO observed.

### 3.2.7 Phthalocyanine-modified electrodes

A 0.08 mM solution of **Co-TAP** or **Ni-TAP** in DMF 50  $\mu\text{L}$  was throughoutly dropped on **Electrode 1 – Electrode 6** and the electrodes were dried at 50  $^{\circ}\text{C}$  in open air. This dropcasting process was repeated 3 times to obtain the phthalocyanine-modified **Electrode 1-Electrode 6**.

### 3.2.8 Electropolymerization of phthalocyanine monomers

The electropolymerization was performed by means of the CV in the three-electrode one-compartment setup consisting of **Electrode 1-Electrode 6** as the WE, the platinum plate as the CE and the Ag/AgCl QRE. A 0.1 M TBAPF<sub>6</sub> solution in DMF was used as a supporting electrolyte and contained 0.8 mM **Co-TAP** or **Ni-TAP**. The solution was purged with N<sub>2</sub> for 10 min prior to the polymerization that was carried out at a potential swept between -0.70 V and 0.90 V vs. Ag/AgCl QRE at the scan rate of 50  $\text{mV}\cdot\text{s}^{-1}$  for 20 cycles. Then, the resulting phthalocyanine-coated WE was removed from the solution and rinsed with DMF and acetone.

### 3.3 Preliminary investigation on energy storage performance of the prepared electrodes

As shown in **Figure 3-1**, active surface area calculation, the CV and GCD were performed in the three-electrode one-compartment setup consisting of **Electrode 1-Electrode 6** as the WE, the platinum plate as the CE and the Ag/AgCl QRE. The supporting electrolyte for each technique is described below.

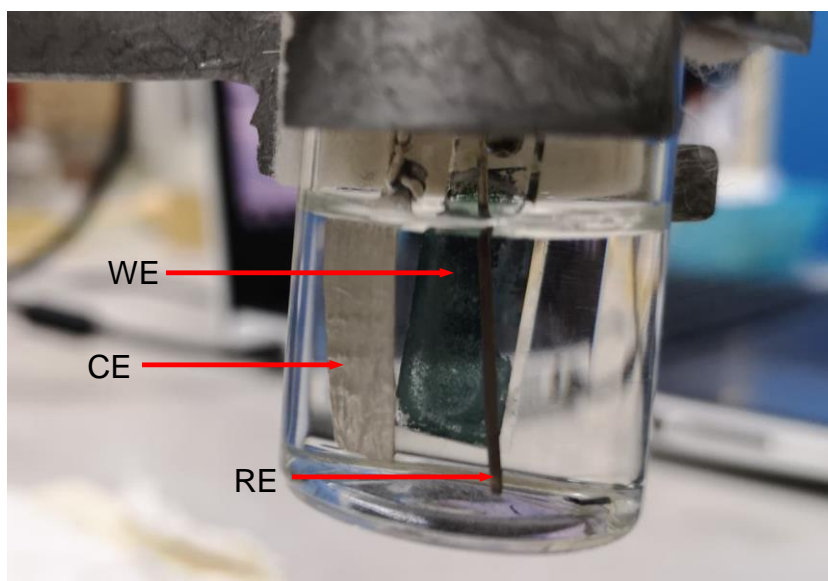


**Figure 3-1.** Electrochemical set up for active surface area calculation, CV and GCD.

### 3.3.1 Determination of active surface area of the prepared electrodes by CV and Randles Sevcik equation

To calculate the active surface area of the prepared electrode. CV was carried out in the electrochemical setup as shown in **Figure 3-1** in a 1.0 M KCl aqueous solution containing 5.0 mM ferrocyanide as the supporting electrolyte in a potential range of  $-0.20$  V to  $0.60$  V vs. Ag/AgCl QRE at the scan rate of 5, 10, 30, 50, 100, 150 and  $200 \text{ mV}\cdot\text{s}^{-1}$  for 3 cycles each.<sup>57</sup>

### 3.3.2 Investigation on specific capacitance of the prepared electrode by CV

The specific capacitance of the prepared electrodes was studied by using the electrochemical setup as shown in **Figure 3-1** was carried out in a 1.0 M  $\text{KHCO}_3$  aqueous solution in a potential range of  $-0.50$  V to  $0.30$  V vs. Ag/AgCl QRE at the scan rate of  $10 \text{ mV}\cdot\text{s}^{-1}$  for 5 cycles.



### 3.3.3 Investigation on specific capacitance of the prepared electrode by GCD

The GCD was carried out at the constant current of 0.1, 0.5 and 1.0 mA•cm<sup>-2</sup> with potential cut-off at -0.50 V and 0.30 V vs. Ag/AgCl QRE for 1 cycle in the 1.0 M KHCO<sub>3</sub> aqueous solution.

### 3.3.4 Sodium-ion battery based on the phthalocyanine-based electrode

As shown in **Figure 3-2**, the sodium-ion battery was fabricated in an 'EL-CELL' electrochemical test equipment consisting of the phthalocyanine-based electrode as the WE, sodium foil (diameter = 17 mm) as the CE, sodium ingot (diameter = 0.3 to 0.8 mm) as the RE, 1.0 M sodium bis(fluorosulfonyl)imide (NaFSI) in 1:1 dimethyl carbonate: ethylene carbonate as the supporting electrolyte and a fiber glass as a separator. The setup diagram of the 'EL-CELL' is shown in **Figures 3-2** and **3-3**.

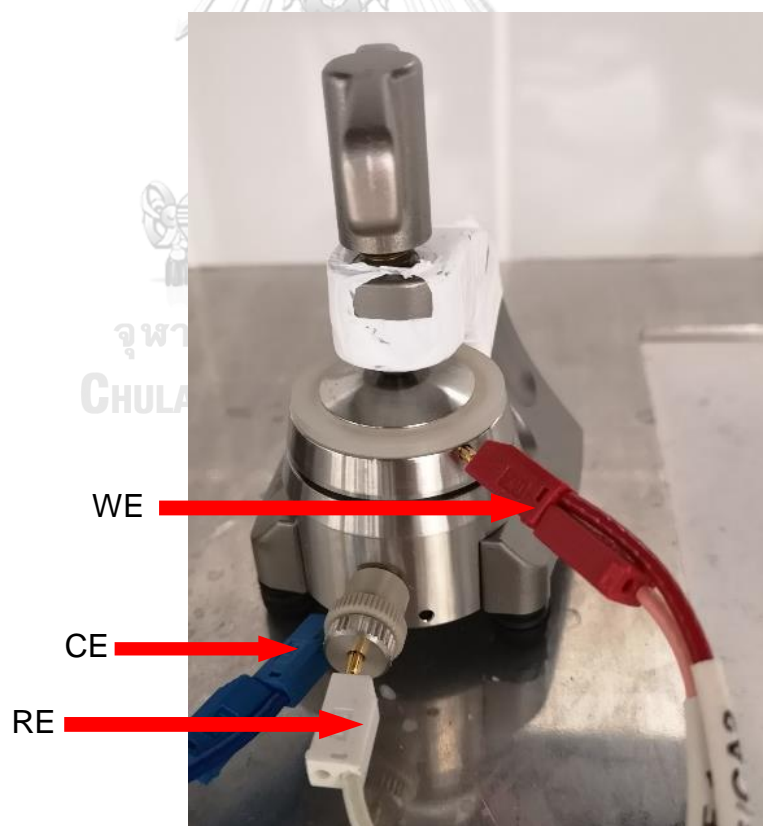


**Figure 3-2.** Electrochemical setup for sodium-ion battery

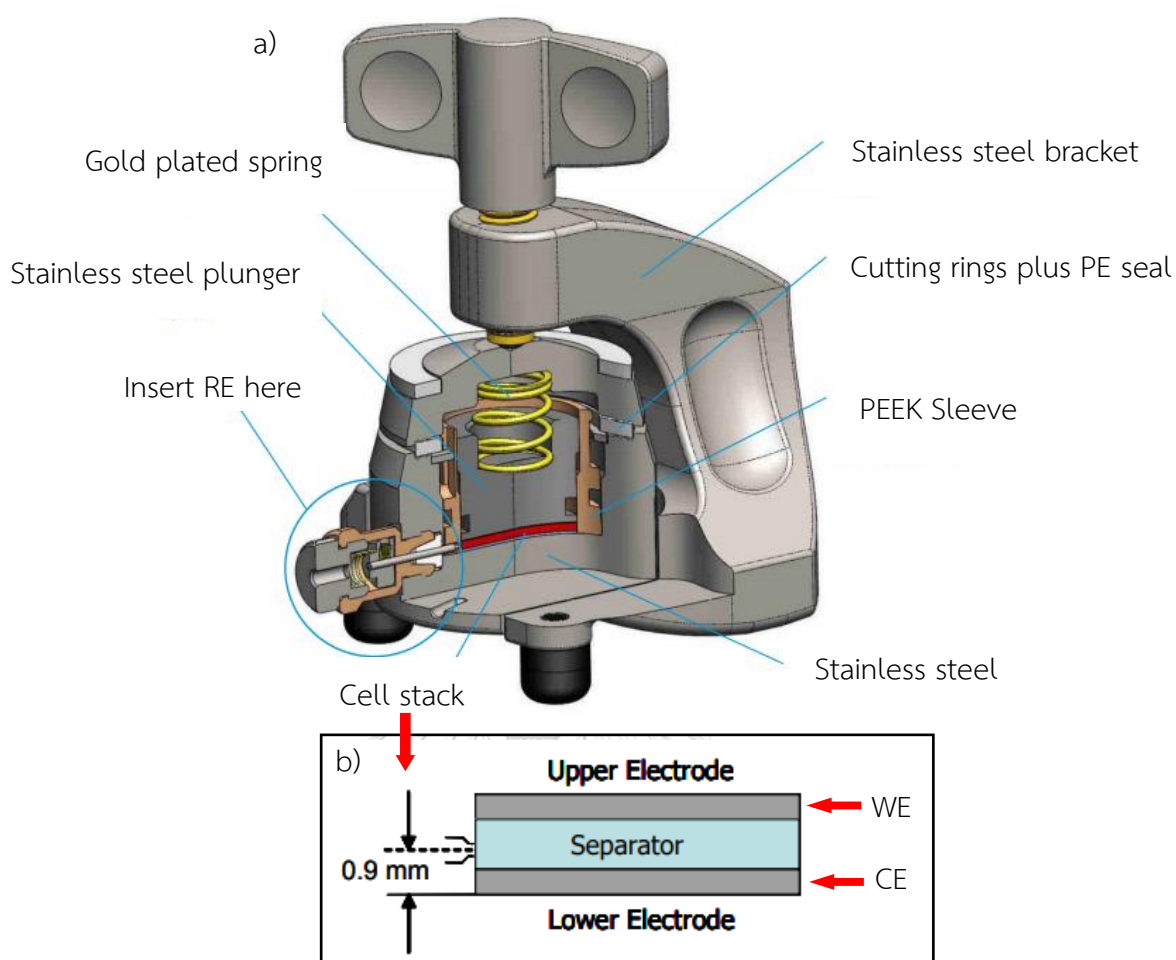


Figure 3-3. a) Setup diagram of 'EL-CELL' and b) schematic cell stack<sup>58</sup>

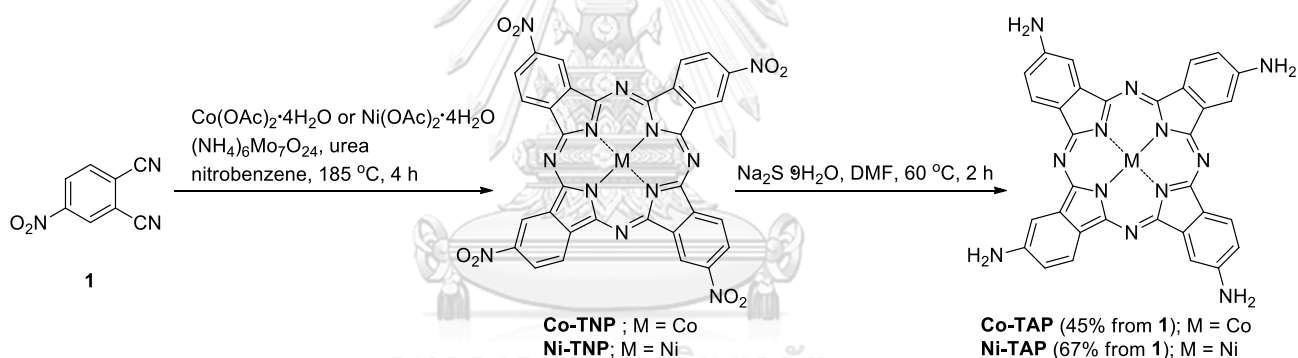
The resulted sodium-ion battery was investigated by means of the CV in the potential range of 1.00 V to 3.00 V vs. Na/Na<sup>+</sup> at the scan rate of 50, 20, 10, 5, 2, 1, 0.5 and 0.1 mV•s<sup>-1</sup> for 5 cycles each. The potential values were reported with respect to the Na. Consequently, GCPL experiment was carried out between 1.00 V and 3.00 V vs. Na/Na<sup>+</sup> at the constant current rates (C-rates) of 3.94 μA (C/10), 19.7 μA (C/2), 39.4 μA (1C), 78.8 μA (2C), 197 μA (5C), 394 μA (10C), 2.36 mA (60C) for 15 cycles each and then at 3.94 μA (C/10 2<sup>nd</sup> time) again for 20 cycles.

## CHAPTER IV

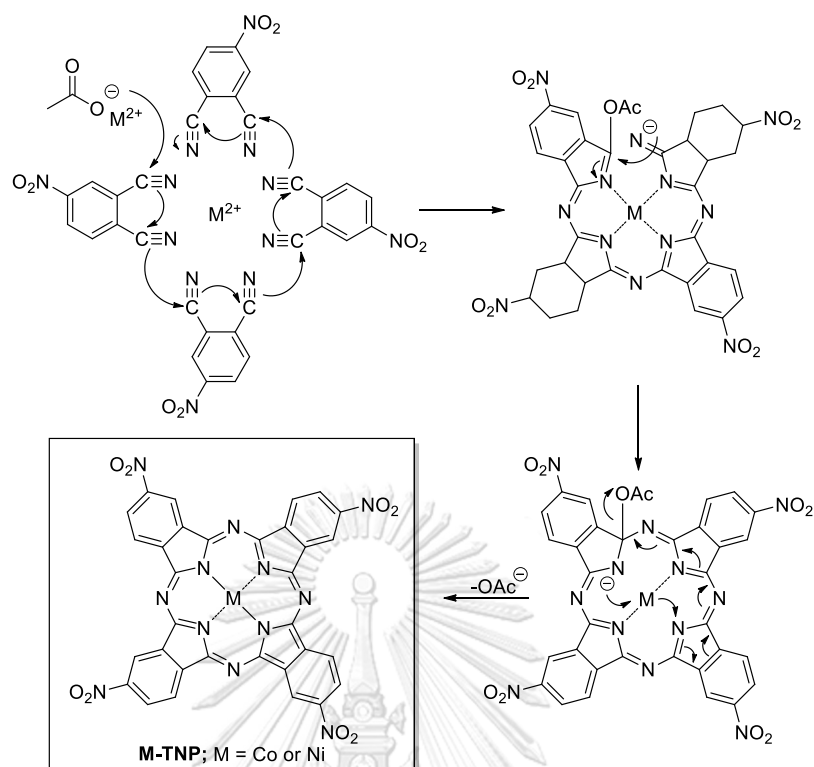
### RESULTS AND DISCUSSION

#### 4.1 Synthesis and characterization of the target phthalocyanines

Synthesis of **Co-TNP** and **Ni-TNP** started from the phthalocyanine ring formation by a reaction of 4-nitroptalonitrile under catalysis of ammonium molybdate in the presence of urea and simultaneous metalation with cobalt(II) acetate tetrahydrate or nickel(II) acetate tetrahydrate as shown in **Scheme 4-1**.<sup>59</sup> Assistance from a nucleophilic acetate anion was required to initiate the cyclization as shown in **Scheme 4-2**.<sup>60</sup> After that, the resulting nitro-containing phthalocyanines were subjected to reduction by using sodium sulfide nonahydrate, leading to **Co-TAP** and **Ni-TAP** in 45% and 67% overall yield, respectively.



**Scheme 4-1.** Synthesis of tetraaminometallophthalocyanines



**Scheme 4-2.** Formation of tetranitrometallophthalocyanine

The successful formation of these two compounds was confirmed by the MALDI-TOD-MS showing for their molecular ion peaks at  $m/z$  631.227 for **Co-TAP** and 630.174 for **Ni-TAP** as shown in **Figure S1** and **Figure S2**. The absorption spectra of **Co-TAP** and **Ni-TAP**, as shown in **Figure S3** and **S4**, collected in DMF exhibited similar features having characteristic Q bands at 719–721 nm with shoulders at 647–648 nm, corresponded to  $\pi$ - $\pi^*$  transition,<sup>61</sup> broad absorption bands at 411–427 nm, which come from metal to ligand charge transfer, and characteristic Soret bands (B bands) at 311–322 nm, arising from  $n$ - $\pi^*$  transition. These mass and absorption spectra are consistent with those described in previous reports.<sup>62,63,64</sup>

## 4.2 Synthesis and characterization of TNT

TNT was obtained from autoclaving  $\text{TiO}_2$  anatase powder in a 10.0 M NaOH aqueous solution at 135 °C for 24 h.<sup>53</sup> Upon the hydrothermal treatment, a lamellar structure of  $\text{Na}_2\text{Ti}_2\text{O}_3\cdot\text{H}_2\text{O}$ , which was believed to be an intermediate for nanotube formation, was generated. After adjusting the pH to 7 by 1.0 M HCl,  $\text{H}^+$  from acid substituted the  $\text{Na}^+$  and changed the lamellar structure into titanate nanotubes.<sup>65</sup> TEM images of the resulting TNT in **Figures 4-1** showed the nanotube structure of the resulting TNT with the width and the length of approximately 10 nm and 200 nm, respectively.

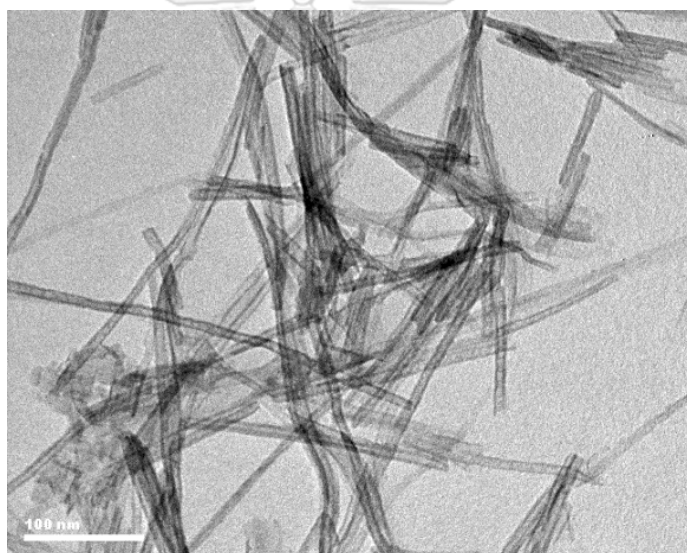


**Figure 4-1.** A TEM image of TNT

## 4.3 Preparation of phthalocyanine-modified electrodes

In this study, the ITO-coated glass was used as a base substrate and assigned as **Electrode 1**. TNT was coated on the ITO-coated glass in order to improve conductivity and surface area of the electrode, resulting in **Electrode 2**.<sup>39</sup> PEDOT was introduced on **Electrode 1** and **Electrode 2** to improve conductive properties to give **Electrode 3** and **Electrode 5**, respectively.<sup>45</sup> To further enhance the conductivity and the surface area of the electrodes,<sup>46</sup> rGO was simultaneously deposited on **Electrode 1** and **Electrode 2** with PEDOT leading to **Electrode 4** and **Electrode 6**, respectively.

In summary, the compounds of each kind of electrode are listed as the following:

**Electrode 1** ITO-coated glass

**Electrode 2** TNT/ITO-coated glass

**Electrode 3** PEDOT/ITO-coated glass

**Electrode 4** PEDOT-rGO/ITO-coated glass

**Electrode 5** PEDOT/TNT/ITO-coated glass

**Electrode 6** PEDOT-rGO/TNT/ITO-coated glass

Then, 4 types of the phthalocyanines, **Co-TAP**, **poly(Co-TAP)**, **Ni-TAP** and **poly(Ni-TAP)** were coated onto those electrodes, resulting in a total of 24 phthalocyanine-modified electrodes which were investigated for their capacitive properties and energy storage performance in comparison to the above-mentioned 6 kinds of electrodes.

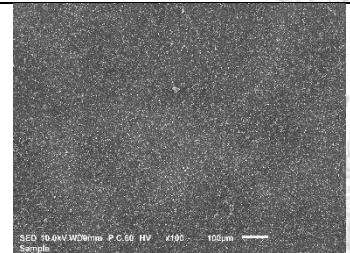
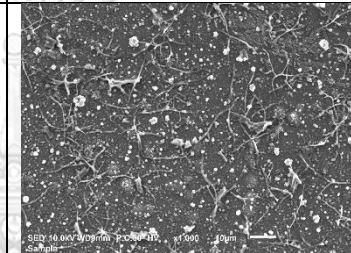
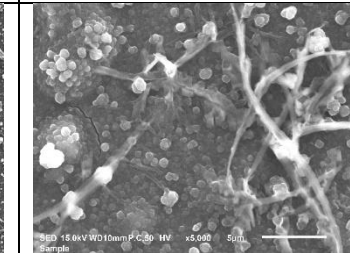
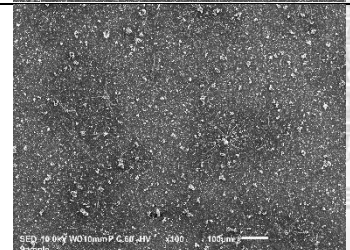
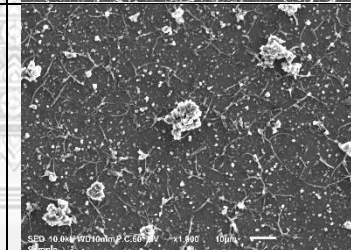
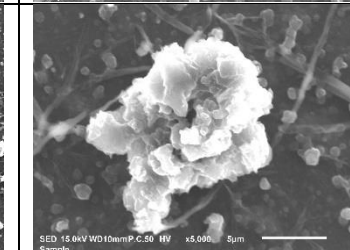
#### 4.3.1 Electrochemical deposition of PEDOT and PEDOT-rGO

In this study, the electrochemical deposition of PEDOT was performed by chronoamperometry in the one-compartment three-electrode setup consisting of **Electrode 1** or **Electrode 2** as the WE, the platinum plate as the CE and the Ag/AgCl QRE, all of which were immersed in the 0.1 M H<sub>2</sub>SO<sub>4</sub> aqueous solution containing 0.01 M EDOT.<sup>55</sup> The electropolymerization of EDOT was carried out at the constant potential of 0.90 V vs. Ag/AgCl for 5 min. This potential initiated the electrochemical oxidation of EDOT by generating EDOT radical cation.<sup>66</sup> Two EDOT radical cations then dimerized together, followed by proton deprotonation with assistance of water to obtain a dimer. After repetition of this step for n times, the polymeric PEDOT film was formed on **Electrode 1** and **Electrode 2** to give **Electrode 3** and **Electrode 5**, respectively.

In a similar manner, when the 0.1 M electrolyte solution H<sub>2</sub>SO<sub>4</sub> contained 0.01 M of EDOT and 1 mg·mL<sup>-1</sup> of GO, both oxidation of EDOT and reduction of GO to rGO<sup>49</sup> could occur simultaneously. The dark blue films of PEDOT and rGO were formed on **Electrode 1** and **Electrode 2**, and became new substrates for the phthalocyanine, *i.e.* **Electrode 4** and **Electrode 6**, respectively. After the electrochemical deposition process, the morphology of the resulting electrodes was investigated by the SEM to

confirm the presence of PEDOT and PEDOT-rGO. The results in **Table 4-1** clearly showed a small grain structure of PEDOT<sup>67</sup> on **Electrode 3** and agglomeration of PEDOT on **Electrode 4**. This agglomeration indicated that the polymerization of PEDOT occurred on the surface of rGO owing to the  $\pi$ - $\pi$  interaction and hydrogen bond between PEDOT and rGO.<sup>68</sup>

**Table 4-1.** SEM images of **Electrode 3** and **Electrode 4** at 100, 1000 and 5000 magnification

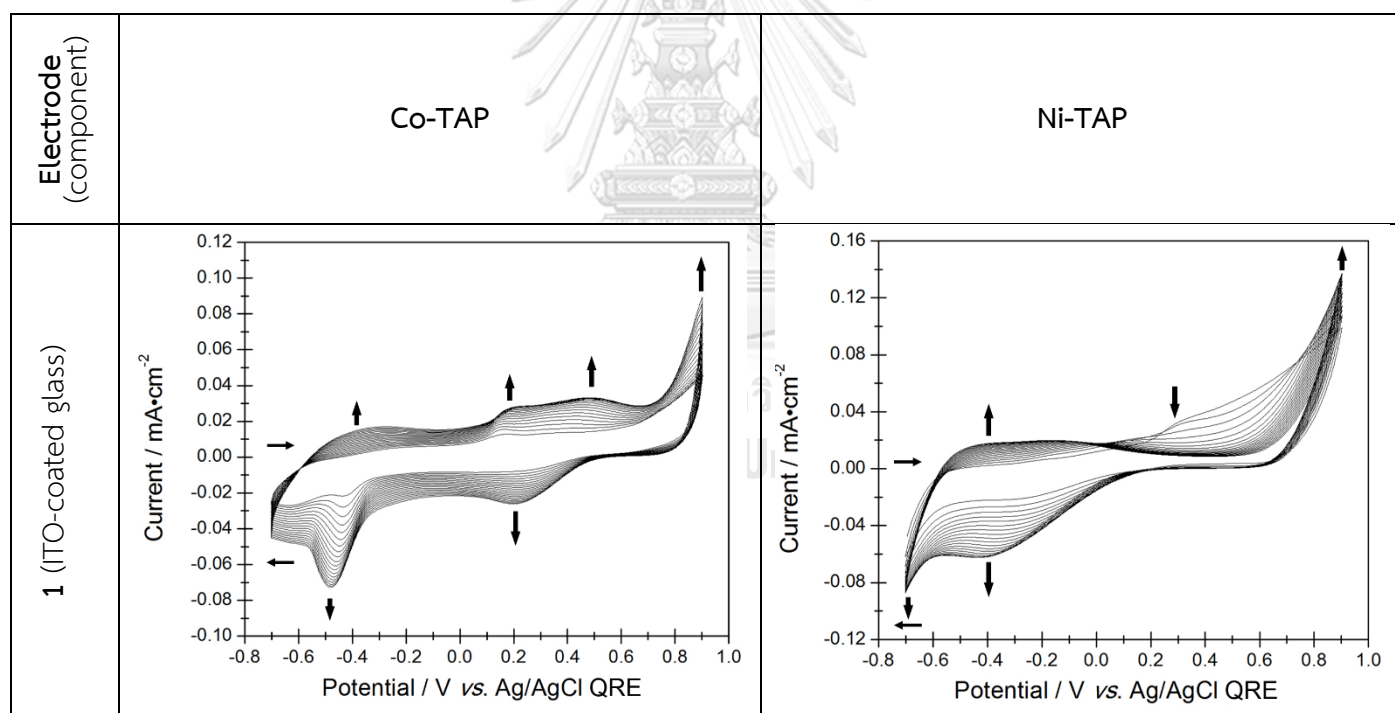
Electrode (component)	Magnification		
	100	1000	5000
<b>3</b> (PEDOT/ ITO-coated glass)			
<b>4</b> (PEDOT-rGO/ ITO-coated glass)			

#### 4.3.2 Electropolymerization of phthalocyanine monomers

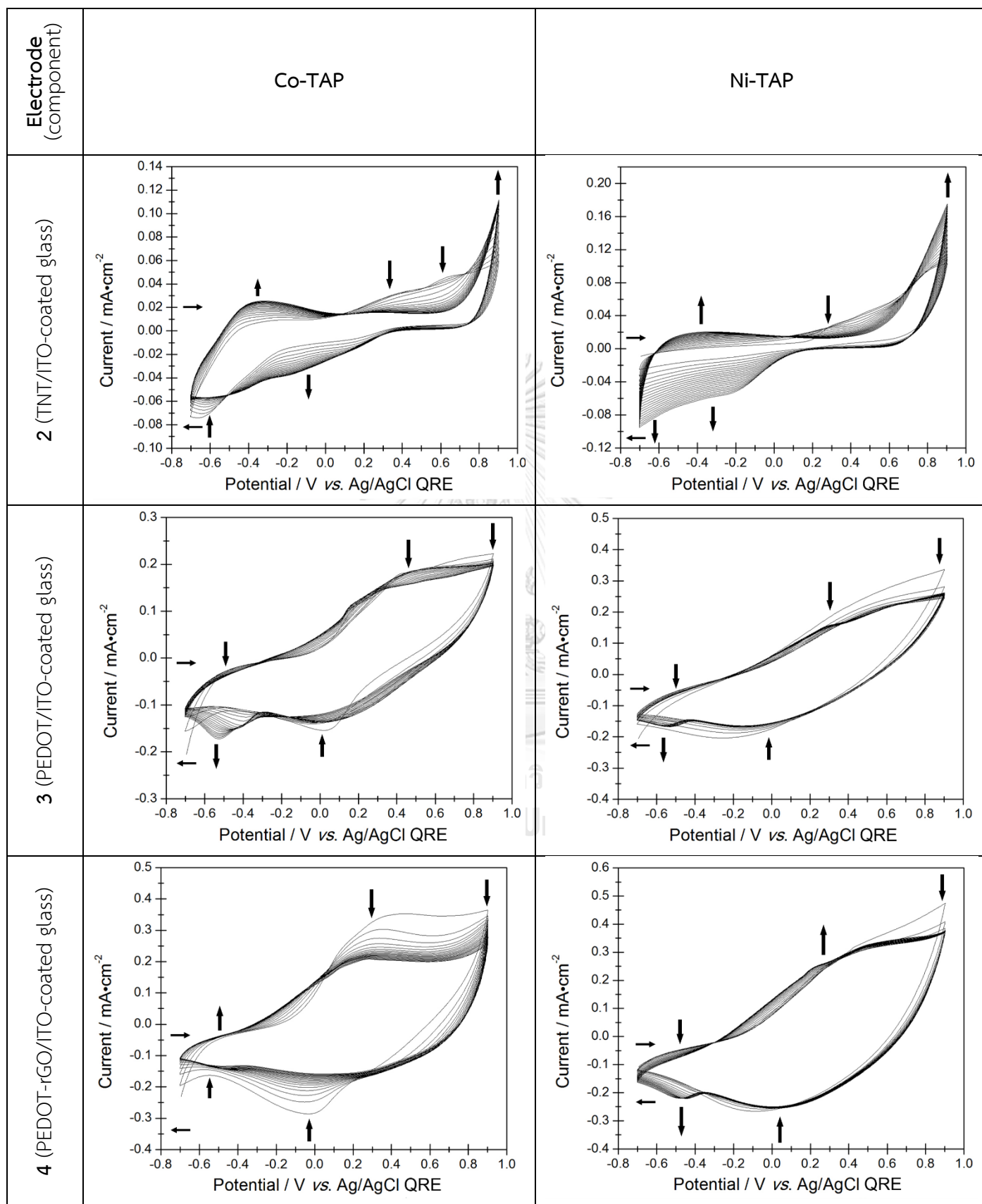
The electropolymerization of **Co-TAP** and **Ni-TAP** was performed by means of the CV using a one-compartment three-electrode setup consisting of **Electrode 1-Electrode 6** as the WE, the platinum plate as the CE and the Ag/AgCl QRE. Cyclic voltammograms were recorded in DMF containing 0.1 M TBAPF<sub>6</sub> and 0.8 mM monomer under N<sub>2</sub> atmosphere at the potential ranging from -0.70 V to 0.90 V vs. Ag/AgCl QRE at the scan rate of 50 mV·s<sup>-1</sup> with the number of scanning cycles of 20. All cyclic voltammograms are summarized in **Table 4-2**. The electropolymerization of **Co-TAP** on **Electrode 1** showed three oxidation peaks at peak potentials ( $E_{\text{peak}}$ ) of -0.39 V, 0.48 V and 0.90 V vs. Ag/AgCl QRE in the first cycle, referring to the oxidation of Co<sup>1+</sup> to Co<sup>2+</sup>, Co<sup>2+</sup> to Co<sup>3+</sup> and the amino groups, respectively.<sup>52</sup> Moreover, the current densities of

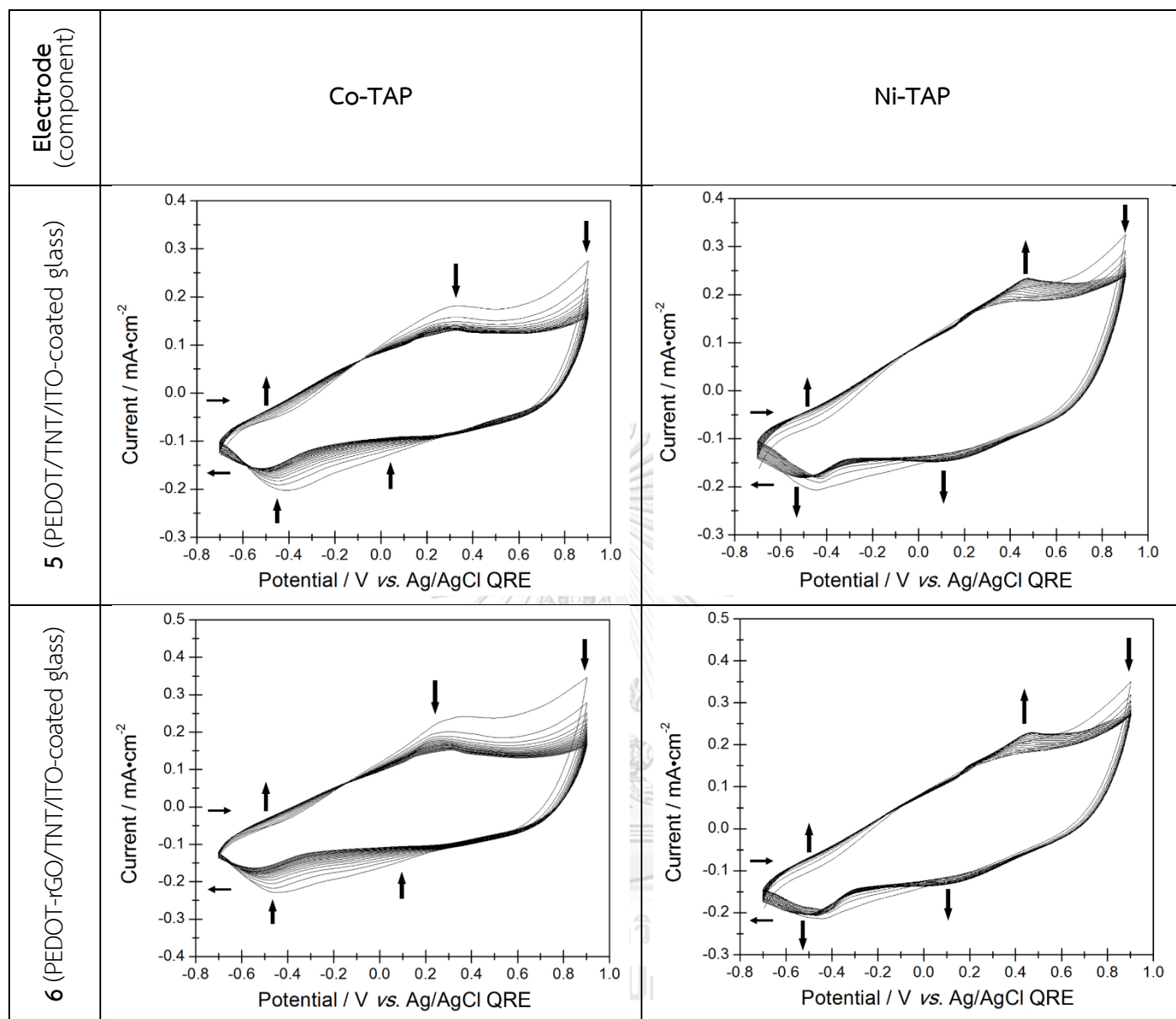
these peaks were increased with the increasing number of cycles and shifted to more positive potentials. A small oxidation peak at  $E_{\text{peak}}$  of 0.18 V was consistent with the previously reported oxidation potential of leucoemeraldine base to emeraldine salt.<sup>69</sup> As for the electropolymerization of Ni-TAP on **Electrode 1** showed three oxidation peaks at  $E_{\text{peak}}$  of -0.40 V, 0.28 V and 0.90 V vs. Ag/AgCl QRE in the first cycle, referring to the oxidation of  $\text{Ni}^{1+}$  to  $\text{Ni}^{2+}$ ,  $\text{Ni}^{2+}$  to  $\text{Ni}^{3+}$  and the amino groups, respectively.<sup>70,71</sup> With the increasing number of cycles, the current density of  $\text{Ni}^{2+}/\text{Ni}^{3+}$  oxidation was decreased but that of the amino group oxidation was increased. These observations indicated a successfully deposition of **poly(Co-TAP)** and **poly(Ni-TAP)** on **Electrode 1**.

**Table 4-2.** Cyclic voltammograms obtained from the electropolymerization of Co-TAP and Ni-TAP on **Electrode 1** to **Electrode 6**









The electropolymerization of **Co-TAP** and **Ni-TAP** on **Electrode 2** gave the similar cyclic voltammograms as that observed from the electropolymerization on **Electrode 1** with slight potential shift to higher potentials. The oxidation peak at 0.90 V vs. Ag/AgCl QRE also showed higher current density due to the higher surface area of TNT, compared with that of the ITO-coated glass,<sup>39</sup> with proportional increase with the increasing number of the scans due to the growth of the polymer film on the electrode surface.<sup>72</sup>

Moreover, the electropolymerization of **Co-TAP** and **Ni-TAP** on **Electrode 1** to give **Electrode 3** showed a characteristic PEDOT redox peak around  $-0.50$  V and  $0.30$  V vs. Ag/AgCl QRE<sup>73</sup> together with the phthalocyanine characteristic redox peaks at  $0.90$  V vs. Ag/AgCl as discussed before. Also, the current density obtained from **Electrode 3** was drastically increased compared with that from **Electrode 1**, likely due to enhanced conductive properties of PEDOT.<sup>45</sup> In addition, the concurrent electropolymerization of EDOT and reduction of GO on **Electrode 1** led to the formation of the blended film of PEDOT and rGO and gave **Electrode 4**. The cyclic voltammograms obtained from this process had similar pattern with higher current density, compared with that observed in the case of **Electrode 3** because of improved electronic transportation and surface area provided by rGO.<sup>46</sup>

In the similar manner, the cyclic voltammograms obtained from the electropolymerization of **Co-TAP** and **Ni-TAP** on **Electrode 5** and **Electrode 6** had consistent patterns as those observed in the case of **Electrode 3** and **Electrode 4**, respectively, as shown in **Figure S5**.

#### 4.4 Preliminary studies on specific capacitance of the phthalocyanine-based electrodes

To determine the specific capacitance, electrochemically active surface areas of phthalocyanine-based electrodes were calculated from their cyclic voltammogram by Randles Sevcik equation as follow:<sup>58</sup>

$$i_p = 268,600 n^{\frac{3}{2}} A^{\frac{1}{2}} D^{\frac{1}{2}} C v^{\frac{1}{2}} \quad (3)$$

- where  $i_p$  = current maximum (A)  
 $n$  = number of electrons transferred in the redox reaction  
 $A$  = electrochemically active surface area (cm<sup>2</sup>)  
 $D$  = diffusion coefficient (cm<sup>2</sup>•s<sup>-1</sup>)  
 $C$  = concentration (mol•cm<sup>-3</sup>)  
 $v$  = scan rate (V•s<sup>-1</sup>)

The CV was carried out in the three electrode one-compartment cell consisting of the phthalocyanine-based electrodes as the WE, the platinum plate as the CE, the Ag/AgCl QRE and a 1.0 M potassium chloride (KCl) aqueous solution containing 5.0 mM ferrocyanide ( $K_4Fe(CN)_6$ ) as the supporting electrolyte. The cyclic voltammograms were recorded in the potential range of  $-0.20$  V to  $0.60$  V vs. Ag/AgCl QRE for 3 cycles. The cyclic voltammograms of the prepared electrodes are shown in **Figure S6** to **Figure S11**.

As shown in **Table 4-3**, the comparison of **Electrode 1** vs. **Electrode 2**, **Electrode 3** vs. **Electrode 5** and **Electrode 4** vs. **Electrode 6** suggested that the presence of TNT did not significantly affect the electrochemically active surface area of the electrodes. Similarly, same effect was observed when the rGO was introduced to **Electrode 3** and **Electrode 5** to become **Electrode 4** and **Electrode 6**, respectively. However, the results clearly showed that the addition of PEDOT on **Electrode 1** and **Electrode 2** led to great increase in the electrochemically active as observed in **Electrode 3** and **Electrode 5**, respectively. The highest surface area of  $0.5142$  cm<sup>2</sup> was obtained from **Electrode 3**. Moreover, the results revealed that the coating of the phthalocyanine monomers on each electrode did not significantly change the surface area of the electrodes, whereas the polymerization of such monomers on the electrodes tended to decrease the electrochemically active surface area of the resulting electrodes.

**Table 4-3.** Electrochemical active surface area of the unmodified and phthalocyanine-modified electrodes

Electrode (component)	Electrochemical active surface area / cm <sup>2</sup>				
	unmodified	Co-TAP	poly(Co-TAP)	Ni-TAP	poly(Ni-TAP)
<b>1</b> (ITO-coated glass)	0.2533	0.2109	0.0702	0.2331	0.0210
<b>2</b> (TNT/ITO-coated glass)	0.2660	0.1943	0.0821	0.1836	0.0264
<b>3</b> (PEDOT/ITO-coated glass)	0.5142	0.5245	0.3857	0.6628	0.2225
<b>4</b> (PEDOT-rGO/ITO-coated glass)	0.3115	0.3173	0.2571	0.3756	0.1915
<b>5</b> (PEDOT/TNT/ITO-coated glass)	0.3576	0.3385	0.2826	0.3847	0.2810
<b>6</b> (PEDOT-rGO/TNT/ITO-coated glass)	0.3304	0.3290	0.2776	0.3556	0.1646

After the calculation of the electrochemically active surface area, the preliminary determination of the specific capacitance of the prepared electrodes were performed by means of the CV in the same three-electrode one-compartment cell using a 1.0 M KHCO<sub>3</sub> electrolyte solution in the potential range of -0.50 V to 0.30 V vs. Ag/AgCl QRE at the scan rate of 10 mV/s for 5 cycles. **Figure 4-2** presents the cyclic voltammograms of all phthalocyanine-modified and unmodified electrodes. The peak areas of these cyclic voltammograms were used to calculate the specific capacitance per unit surface area according to equation (1). The resulting specific capacitance are summarized in **Table 4-4**. **Figure 4-2a** and **Figure 4-2b** showed that **Electrode 1** and **Electrode 2** originally gave low current density, but in presence of the phthalocyanine polymer films significant increase in the current density was observed. The further enhancement of the current densities could be obtained by introducing the PEDOT and PEDOT-rGO films on the electrodes as shown in **Figure 4-2c** to **Figure 4-2f**. Moreover, the monomer-modified electrodes exhibited high current density in cases of **Electrode 3** and **Electrode 4**, while the polymer-modified ones exhibited high current density in cases of **Electrode 5** and **Electrode 6**.

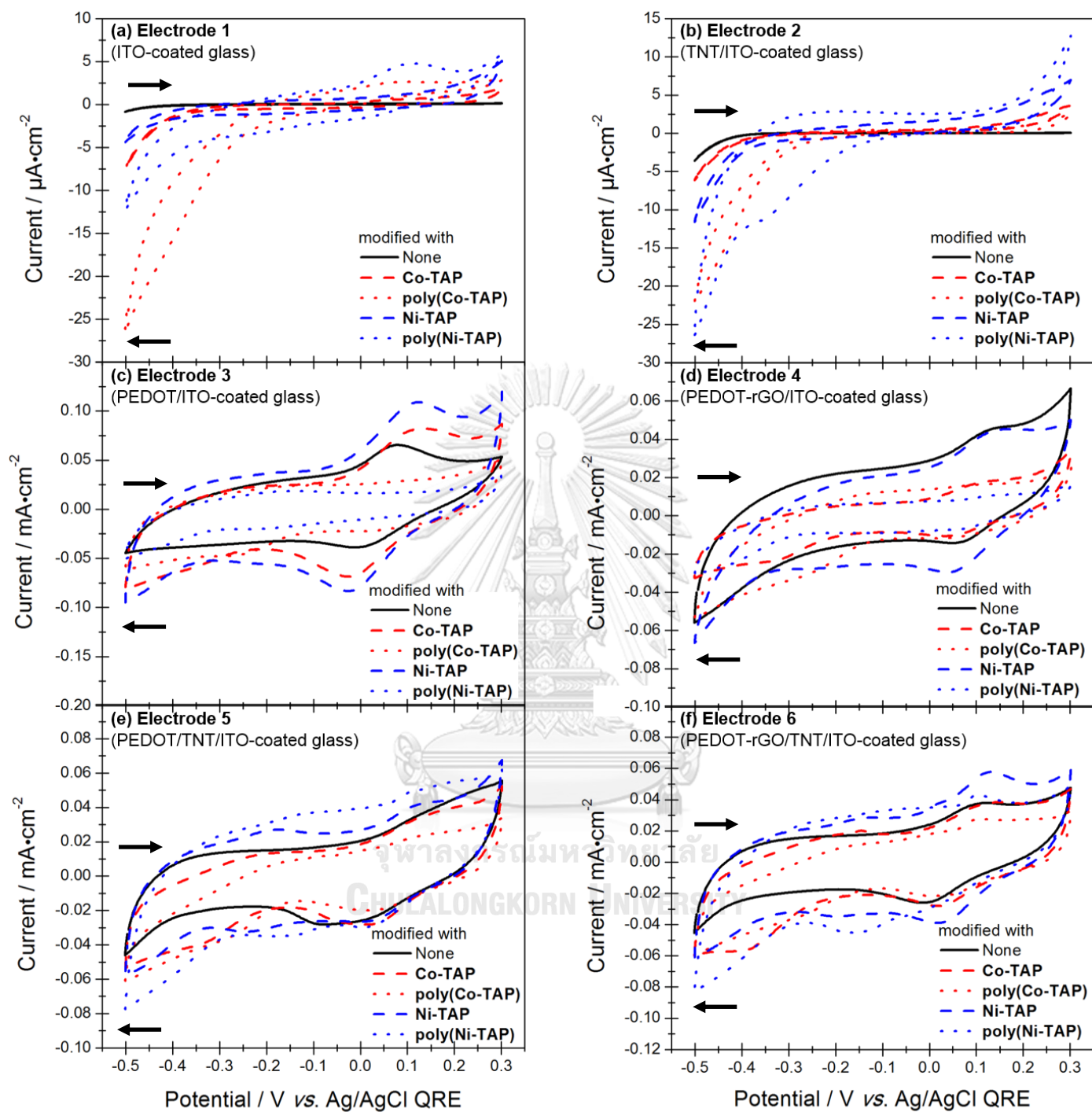


Figure 4-2. Cyclic voltammograms of all phthalocyanine-modified and unmodified electrodes

**Table 4-4.** Specific capacitance of the unmodified and phthalocyanine-modified electrodes determined by CV method

Electrode (component)	Specific capacitance / $\text{mF}\cdot\text{cm}^{-2}$				
	unmodified	Co-TAP	poly(Co-TAP)	Ni-TAP	poly(Ni-TAP)
<b>1</b> (ITO-coated glass)	0.07	0.84	13.1	1.01	29.4
<b>2</b> (TNT/ITO-coated glass)	0.15	0.97	6.87	2.26	36.1
<b>3</b> (PEDOT/ITO-coated glass)	12.7	16.4	14.2	16.5	15.3
<b>4</b> (PEDOT-rGO/ITO-coated glass)	15.8	7.78	13.8	14.3	9.92
<b>5</b> (PEDOT/TNT/ITO-coated glass)	12.3	13.5	14.9	14.4	24.5
<b>6</b> (PEDOT-rGO/TNT/ITO-coated glass)	12.8	15.2	15.3	17.8	40.1

The results in **Table 4-4** suggested that the presence of the phthalocyanine monomers led to significant increase in the specific capacitance and the phthalocyanine polymer films further increased the specific capacitance for most of electrodes. The comparison of **Electrode 1** vs. **Electrode 2**, **Electrode 3** vs. **Electrode 5** and **Electrode 4** vs. **Electrode 6** indicated that TNT improved the specific capacitance of the electrodes coated with Ni-TAP and its polymer, unlike the ones coated with the Co-chelated derivatives. When comparing **Electrode 1** vs. **Electrode 3** and **Electrode 2** vs. **Electrode 5**, PEDOT significantly increased the specific capacitance of the electrodes except for poly(Ni-TAP)-based ones. Moreover, the comparison of **Electrode 3** vs. **Electrode 4** and **Electrode 5** vs. **Electrode 6** showed that rGO could improve the specific capacitance when used together with TNT, possibly because of hydrogen bonding interaction between rGO and TNT. In overall, the Ni-phthalocyanine-based electrodes tended to give better improvement of the specific capacitance of the electrodes than the Co-phthalocyanine-based one and poly(Ni-TAP)/PEDOT-rGO/TNT/ITO-coated glass or the poly(Ni-TAP)/**Electrode 6** exhibited the best specific capacitance among all electrodes with the value of  $40.1 \text{ mF}\cdot\text{cm}^{-2}$ .

To further investigate the charge/discharge behavior of the electrodes, the GCD method was employed by applying the constant current of 0.1, 0.5 and 1.0 mA•cm<sup>-2</sup> to the electrodes to obtain discharge time for using in the specific capacitance calculation per unit surface area according to equation (2). The specific capacitance values have been summarized in **Table 4-5**. The result reveals that the specific capacitance of the electrodes in each current had the same trends as those observed from the CV method, except that rGO could significantly increase the specific capacitance even without the presence of TNT. Also, the electrode that exhibited the best specific capacitance was **poly(Ni-TAP)/Electrode 6**, which gave 58.3 mF•cm<sup>-2</sup> of the specific capacitance at the constant current of 0.1 mA•cm<sup>-2</sup>. Therefore, the **poly(Ni-TAP)/Electrode 6** was chosen for further study on the battery performance discussed in the next section.

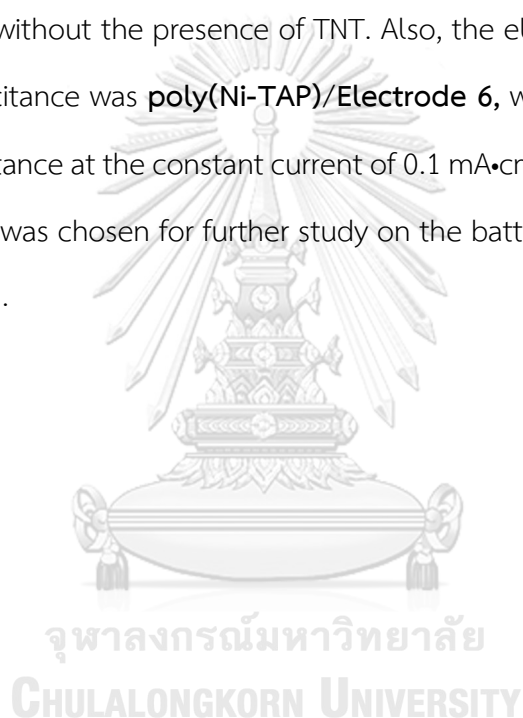




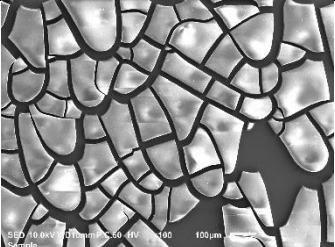
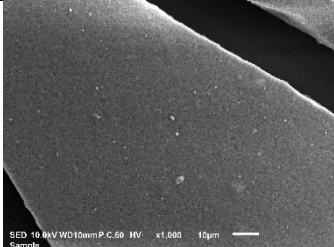
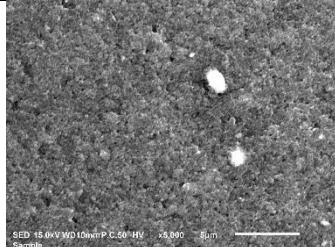
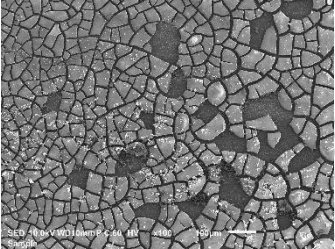
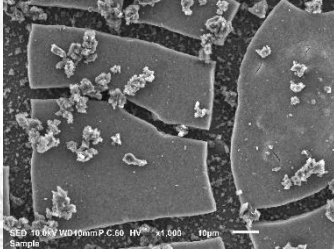
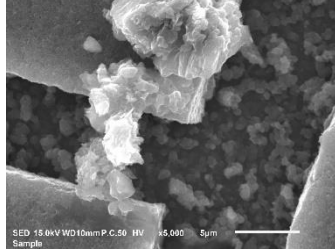
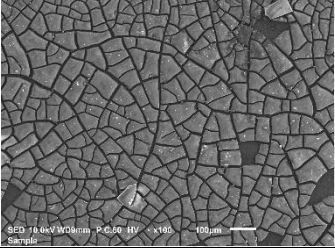
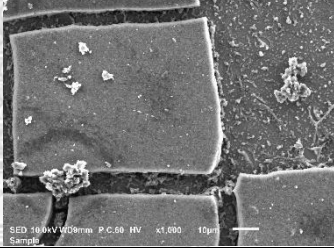
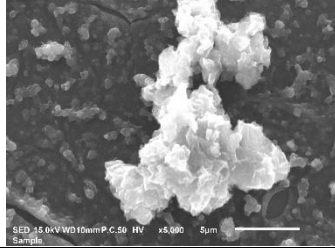
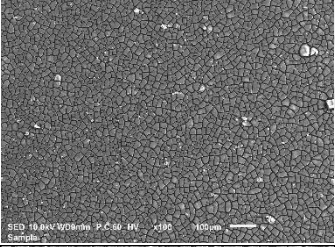
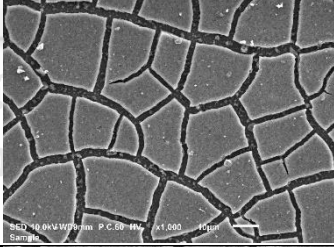
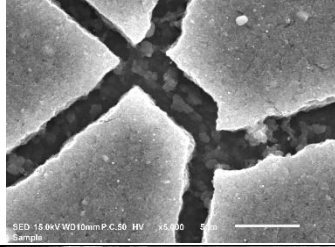
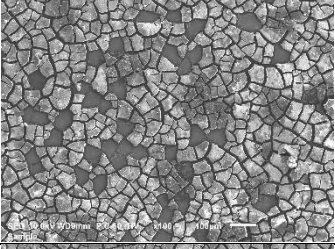
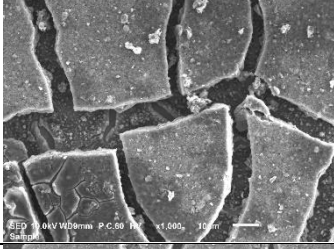
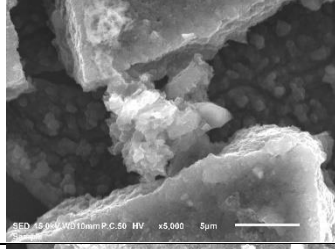
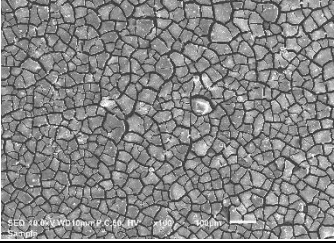
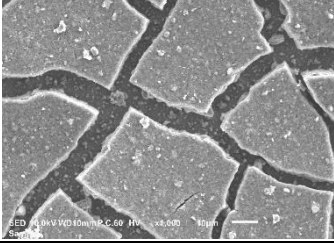
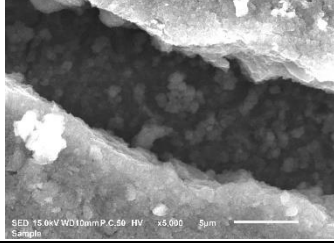
**Table 4-5.** Specific capacitance of the unmodified and phthalocyanine-modified electrodes determined by a GCD method

Electrode (component)	Specific capacitance at 0.1 mA·cm <sup>-2</sup> / mF·cm <sup>-2</sup>				
	unmodified	Co-TAP	poly(Co-TAP)	Ni-TAP	poly(Ni-TAP)
1 (ITO-coated glass)	0.20	0.30	2.00	0.30	38.5
2 (TNT/ITO-coated glass)	0.20	0.70	38.7	0.9	45.0
3 (PEDOT/ITO-coated glass)	28.2	30.9	29.2	29.1	35.0
4 (PEDOT-rGO/ITO-coated glass)	29.4	33.0	32.3	26.7	48.2
5 (PEDOT/TNT/ITO-coated glass)	26.9	28.5	29.3	26.8	52.2
6 (PEDOT-rGO/TNT/ITO-coated glass)	28.7	33.0	43.5	31.0	58.3
Electrode (component)	Specific capacitance at 0.5mA·cm <sup>-2</sup> / mF·cm <sup>-2</sup>				
	unmodified	Co-TAP	poly(Co-TAP)	Ni-TAP	poly(Ni-TAP)
1 (ITO-coated glass)	0.00	0.00	1.30	0.00	20.1
2 (TNT/ITO-coated glass)	0.00	0.60	21.1	0.60	47.9
3 (PEDOT/ITO-coated glass)	8.60	12.8	14.3	13.5	16.5
4 (PEDOT-rGO/ITO-coated glass)	14.0	15.4	18.2	13.8	26.3
5 (PEDOT/TNT/ITO-coated glass)	11.0	13.6	16.3	14.4	44.0
6 (PEDOT-rGO/TNT/ITO-coated glass)	11.9	17.0	18.1	16.9	38.3
Electrode (component)	Specific capacitance at 1.0mA·cm <sup>-2</sup> / mF·cm <sup>-2</sup>				
	unmodified	Co-TAP	poly(Co-TAP)	Ni-TAP	poly(Ni-TAP)
1 (ITO-coated glass)	0.00	0.00	0.90	0.00	25.5
2 (TNT/ITO-coated glass)	0.00	0.00	8.50	0.00	36.0
3 (PEDOT/ITO-coated glass)	8.30	10.0	13.0	12.8	14.0
4 (PEDOT-rGO/ITO-coated glass)	9.50	12.8	15.7	8.8	16.0
5 (PEDOT/TNT/ITO-coated glass)	9.30	11.3	11.3	12.8	32.8
6 (PEDOT-rGO/TNT/ITO-coated glass)	10.5	14.0	13.8	14.8	26.8

SEM images of the unmodified- **Electrode 2** as shown in **Table 4-6** shown sponge-like surface of the TNT over smooth surface of the ITO-coated glass, while the unmodified- **Electrode 6** had grain structure of PEDOT-rGO attached on both of the TNT and the ITO-coated glass. The structure of the both phthalocyanine monomer-modified electrodes consist of phthalocyanine microcrystalline deposited across the ITO-coated glass with the presence of the agglomeration of PEDOT-rGO on the electrodes. In the other hand, the PEDOT-rGO agglomerated structures were lessen the in **poly(Co-TAP)/Electrode 6** and the **poly(Ni-TAP)/Electrode 6**, probably because of structural rearrangement occurred during phthalocyanine electro-polymerization process.



**Table 4-6.** SEM images of unmodified **Electrode 2** and unmodified and phthalocyanine-modified series of **Electrode 6** at 100, 1000 and 5000 magnification

Electrode (component)	Magnification		
	100	1000	5000
unmodified- Electrode 2			
unmodified- Electrode 6			
Co-TAP /Electrode 6			
poly(Co-TAP) /Electrode 6			
Ni-TAP /Electrode 6			
poly(Ni-TAP) /Electrode 6			

#### 4.5 Sodium-ion battery performance

In this study, the sodium-ion battery was fabricated in ‘EL-CELL’ electrochemical test equipment consisting of the phthalocyanine-based electrode as the WE, sodium foil (thickness = 0.3 mm, diameter = 17 mm) as the CE, sodium ingot (thickness = 1.2 mm, diameter = 0.3 mm to 0.8 mm) as the RE, a 1.0 M NaFSI solution in 1:1 dimethyl carbonate:ethylene carbonate as the supporting electrolyte and fiber glass as a separator. Upon application of the potential ranging from of 1.00 V to 3.00 V vs. Na/Na<sup>+</sup> at the scan rate of 50, 20, 10, 5, 2, 1, 0.5 and 0.1 mV·s<sup>-1</sup>, the resulting battery gave the cyclic voltammograms as shown in **Figure 4-3**. By using the scan rate of 50 mV·s<sup>-1</sup> a cathodic desorption of a sodium ion (desodiation) peak at the  $E_{\text{peak}}$  of 2.50 V vs. Na/Na<sup>+</sup> was detected. Upon the reduction of the scan rate, negative shift of the peak with the presence of anodic an insertion of a sodium ion (sodiation) peak at the  $E_{\text{peak}}$  of 1.00 V vs. Na/Na<sup>+</sup> and the decrease in the current of these peaks were observed. This behavior indicated pseudocapacitance properties of the electrode<sup>74</sup> that confirmed intercalation of the sodium-ion on the surface of the electrode.

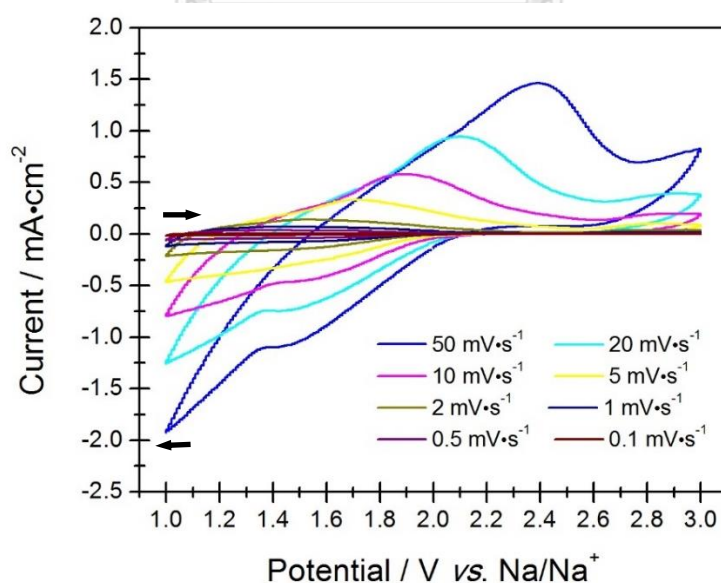


**Figure 4-3.** Cyclic voltammograms of a sodium-ion battery based on a **poly(Ni-TAP)/Electrode 6** at different scan rates in a potential range between 1.00 V and 3.00 V vs. Na/Na<sup>+</sup>

Afterwards, the GCPL experiment was performed at the potential between 1.00 V and 3.00 V vs.  $\text{Na}/\text{Na}^+$  with serial variation of a constant C-rates of C/10, C/2, 1C, 2C, 5C, 10C and 60C for 15 cycles each, and then C/10 as the 2<sup>nd</sup> time for 20 cycles. The charging (desodiation) and discharging (sodiation) responses at different C-rates were presented in the plots between the applied potential and specific capacity as shown in **Figure 4-4**. The results showed that the charging profiles was observed in the potential ranging from 1.80 V to 2.50 V vs.  $\text{Na}/\text{Na}^+$  where the great increase in slope was detected which indicated the desodiation behavior, consistent with the cyclic voltammograms between 1.80 V to 2.50 V vs.  $\text{Na}/\text{Na}^+$  in **Figure 4-3**. The discharging profiles also showed a steady slope in the potential range of 1.00 V to 1.80 V vs.  $\text{Na}/\text{Na}^+$  that reflects the sodiation behavior, which was also observed in its cyclic voltammograms between 1.00 V to 1.80 V vs.  $\text{Na}/\text{Na}^+$ .

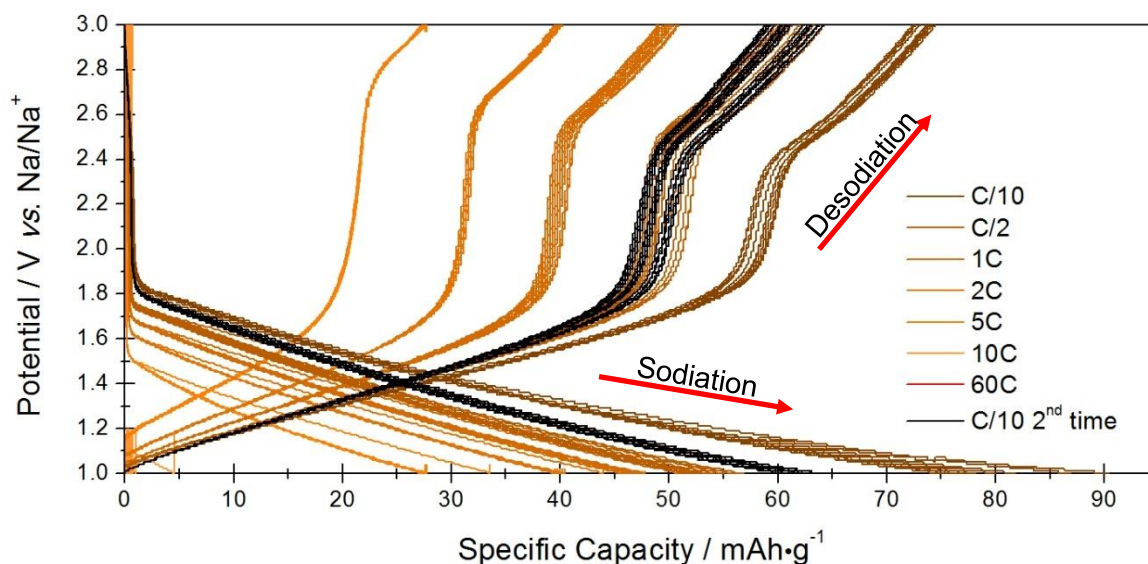


**Figure 4-4.** Galvanostatic charge/discharge curves of a sodium-ion battery at different C-rates between 1.00 V and 3.00 V vs.  $\text{Na}/\text{Na}^+$

To reflect the specific capacity of the charge/discharge process at each cycle number, the plots between the specific capacity and the cycle number as shown in **Figure 4-5** were taken into consideration. The results showed that the galvanostatic charge/discharge cycling at the C-rate of C/10 initially exhibited the specific capacity of  $75.41 \text{ mAh}\cdot\text{g}^{-1}$ . When the C-rate was increased to C/2, the specific capacity was decreased to  $51.61 \text{ mAh}\cdot\text{g}^{-1}$  and then further to  $45.83 \text{ mAh}\cdot\text{g}^{-1}$  at the C-rate of 1C. Moreover, when the C-rates reached 2C and 5C, the specific capacities were decreased to  $39.57 \text{ mAh}\cdot\text{g}^{-1}$  and  $27.55 \text{ mAh}\cdot\text{g}^{-1}$ , respectively. The decrease in the specific capacity indicated the typical behavior of the energy storage system, which resulted from increase in IR-drop when higher current was applied. However, when the C-rates were increased to 10C and 60C, the specific capacity was dropped to nearly  $0 \text{ mAh}\cdot\text{g}^{-1}$ , which meant that this electrode could not be charged and discharged at the high rate. The stability of the sodium-ion battery after 105 cycles was investigated by decreasing the C-rate back to C/10 for 20 cycles. It was found that the sodium-ion battery showed the specific capacity at  $60.22 \text{ mAh}\cdot\text{g}^{-1}$ , equivalent to retention percentage of 79.86%, compared with the initial specific capacity observed at the same C-rate. These observations confirmed that the **poly(Ni-TAP) / Electrode 6** could serve as the electrode for the sodium-ion battery. For possible further investigation and development of the phthalocyanine-based sodium-ion battery, the applied potential range could be extended into more negative region to let more sodium ion insert into the electrode and give more capacity. However, more negative in potential range may cause lowering of materials retention. Thus, the optimum potential range that gives the highest capacity with the satisfactory stability of the electrodes has to be investigated.

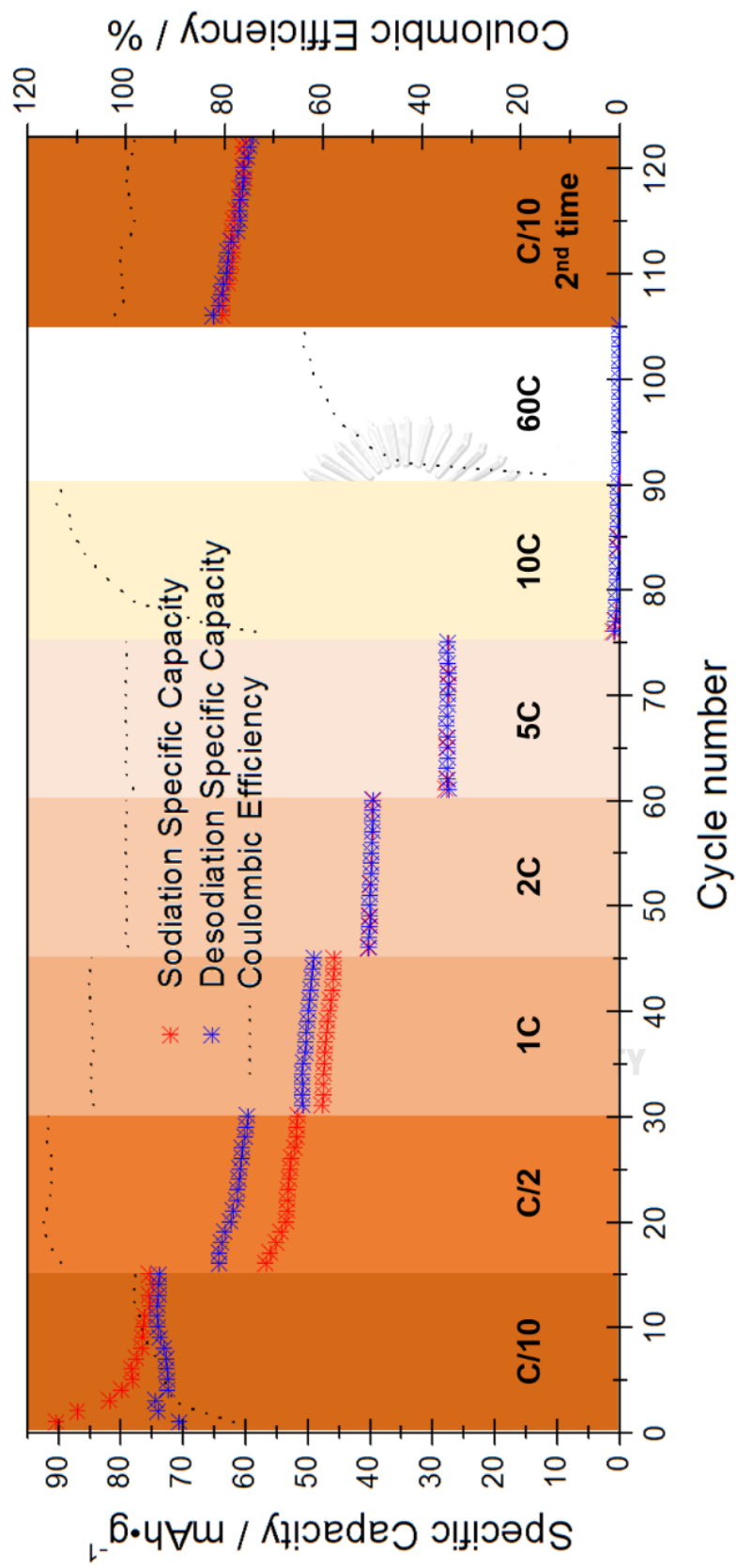


Figure 4-5. Specific capacities of a sodium-ion battery at different C-rates at a potential range between 1.00 V and 3.00 V vs.  $\text{Na}/\text{Na}^+$ .

## CHAPTER V

### CONCLUSION

2,9,16,23-tetraaminophthalocyaninatocobalt(II) (**Co-TAP**) and 2,9,16,23-tetraaminophthalocyaninatonicel(II) (**Ni-TAP**) were synthesized by a reaction of 4-nitrophthalonitrile under catalysis of  $(\text{NH}_4)_6\text{Mo}_7\text{O}_{24}\cdot 4\text{H}_2\text{O}$ , followed by *in-situ* metalation. Reduction of the resulting nitro-substituted phthalocyanines in the presence of  $\text{Na}_2\text{S}$  gave **Co-TAP** and **Ni-TAP** in 45% and 67% overall yield, respectively. The successful formation of the target compound was confirmed by mass spectrometry and UV-visible spectrophotometry. Their monomers were coated and electrochemically polymerized on 6 kinds of the electrodes, namely ITO-coated glass (**Electrode 1**), TNT/ITO-coated glass (**Electrode 2**), PEDOT/ITO-coated glass (**Electrode 3**), PEDOT-rGO/ITO-coated glass (**Electrode 4**), PEDOT/TNT/ITO-coated glass (**Electrode 5**) and PEDOT-rGO/TNT/ITO-coated glass (**Electrode 6**). The preliminary CV and GCD studies of these electrodes showed that both of the phthalocyanine monomers and polymer films increased the specific capacitance of the electrode. The presence of TNT PEDOT and rGO also played significant role in the enhancement of the specific capacitance. Moreover, the Ni-phthalocyanine-based electrodes tended to have higher specific capacitance than the Co-phthalocyanine-based ones and the **poly(Ni-TAP)/Electrode 6** exhibited the highest specific capacitance among all phthalocyanines-based electrodes. The sodium-ion battery based on **poly(Ni-TAP)/Electrode 6** exhibited specific capacity at  $60.22 \text{ mAh}\cdot\text{g}^{-1}$  which obtained at a C-rate of C/10 with retention percentage of 79.86% after 125 cycles.





APPENDIX

จุฬาลงกรณ์มหาวิทยาลัย  
**CHULALONGKORN UNIVERSITY**

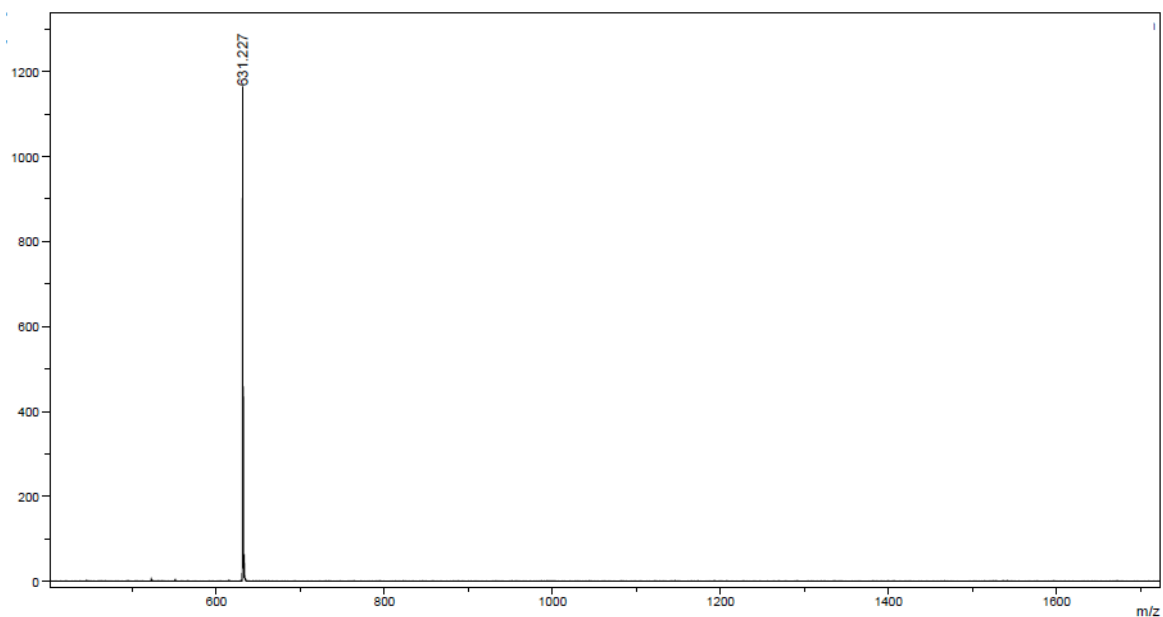


Figure S1. A MALDI-TOF Mass spectrum of Co-TAP

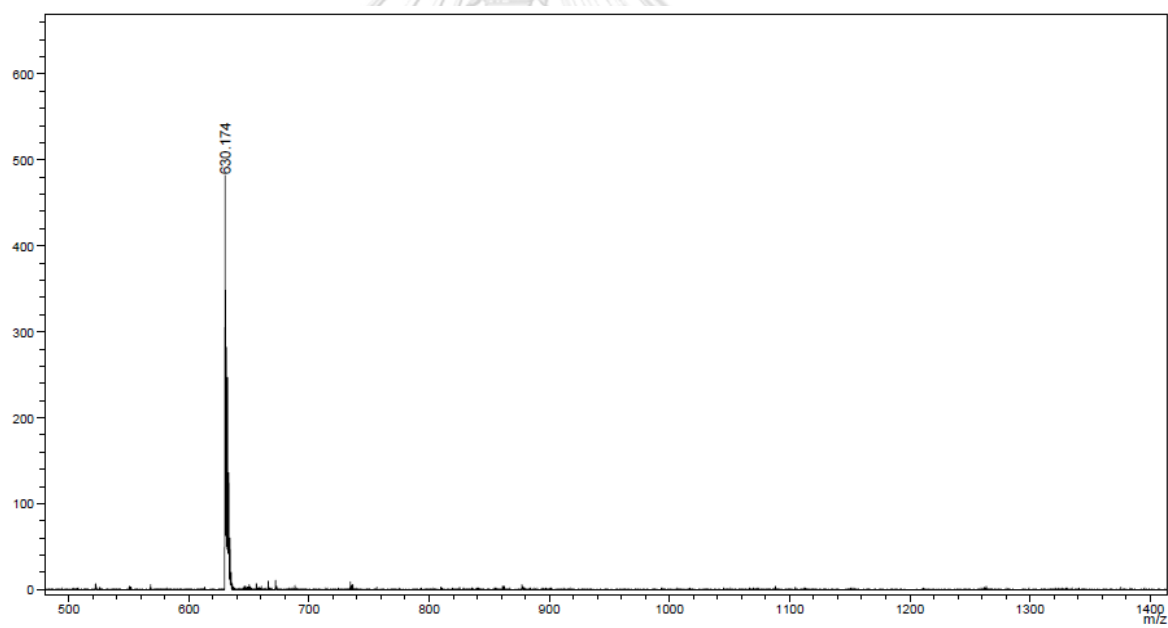


Figure S2. A MALDI-TOF Mass spectrum of Ni-TAP

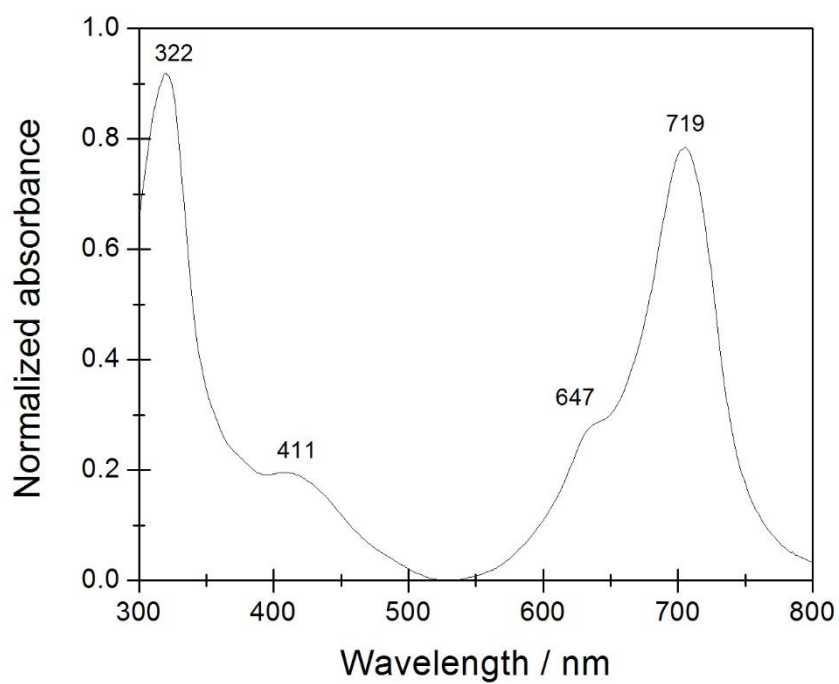


Figure S3. An absorption spectrum of a Co-TAP solution in DMF

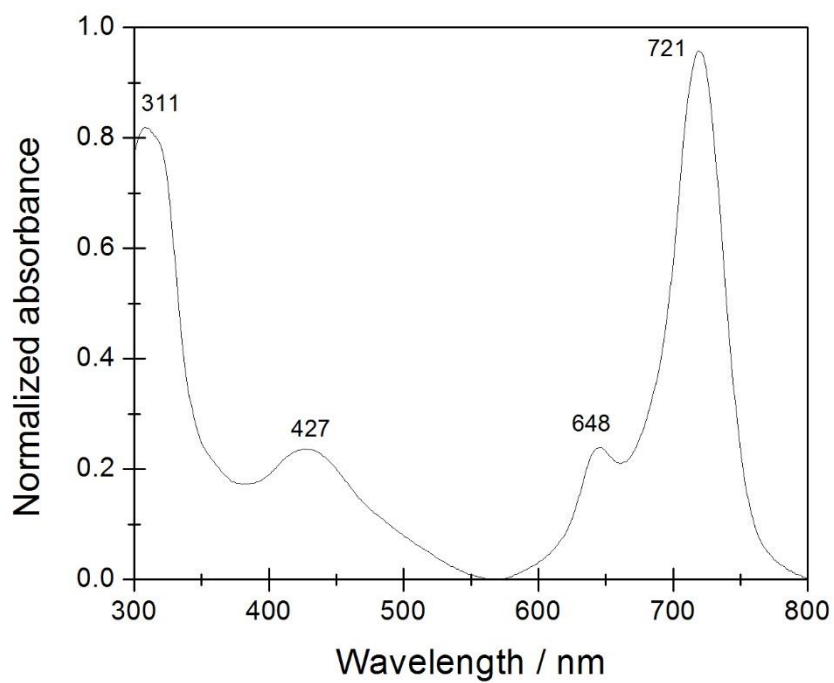
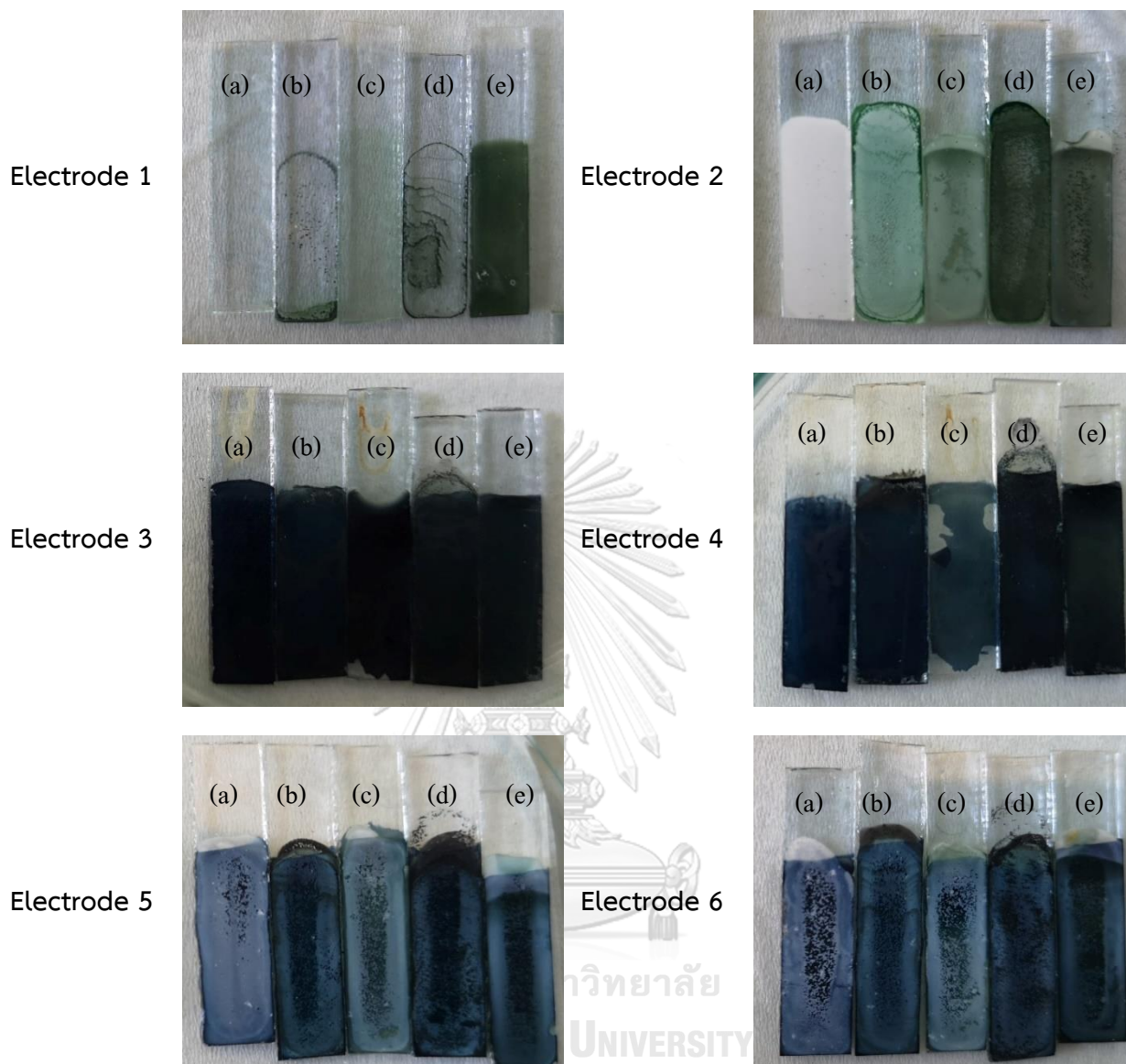
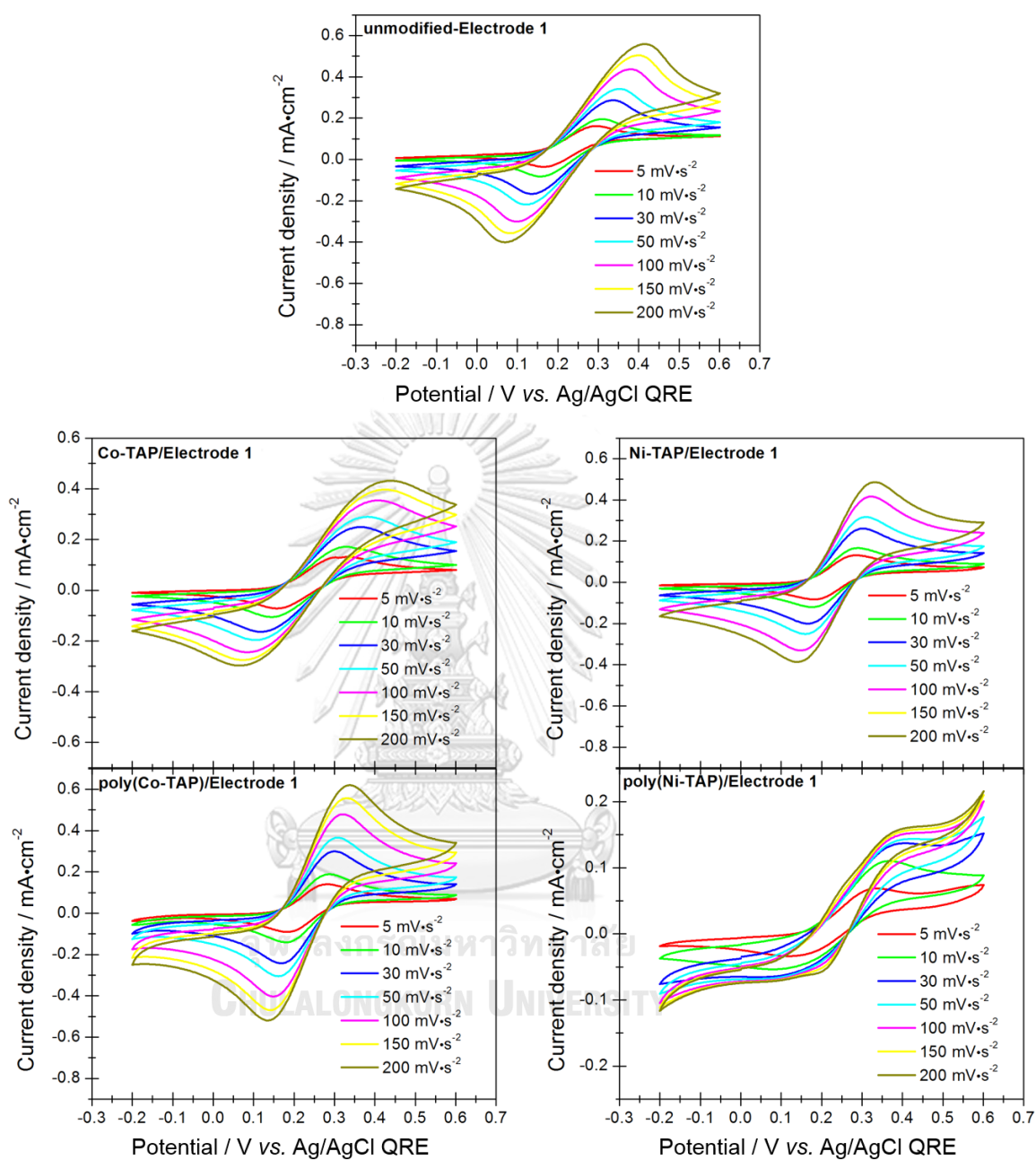


Figure S4. An absorption spectrum of a Ni-TAP solution in DMF



**Figure S5.** Images of the prepared electrode (a) without a phthalocyanine film, and with films of (b) Co-TAP (c) poly(Co-TAP) (d) Ni-TAP (e) poly(Ni-TAP) coated.



**Figure S6.** Cyclic voltammograms of phthalocyanine-modified and unmodified **Electrode 1** in 1.0 M a KCl aqueous solution containing 5.0 mM  $K_4Fe(CN)_6$  at scan rates of 5, 10, 30, 50, 100, 150 and 200  $mV \cdot s^{-1}$

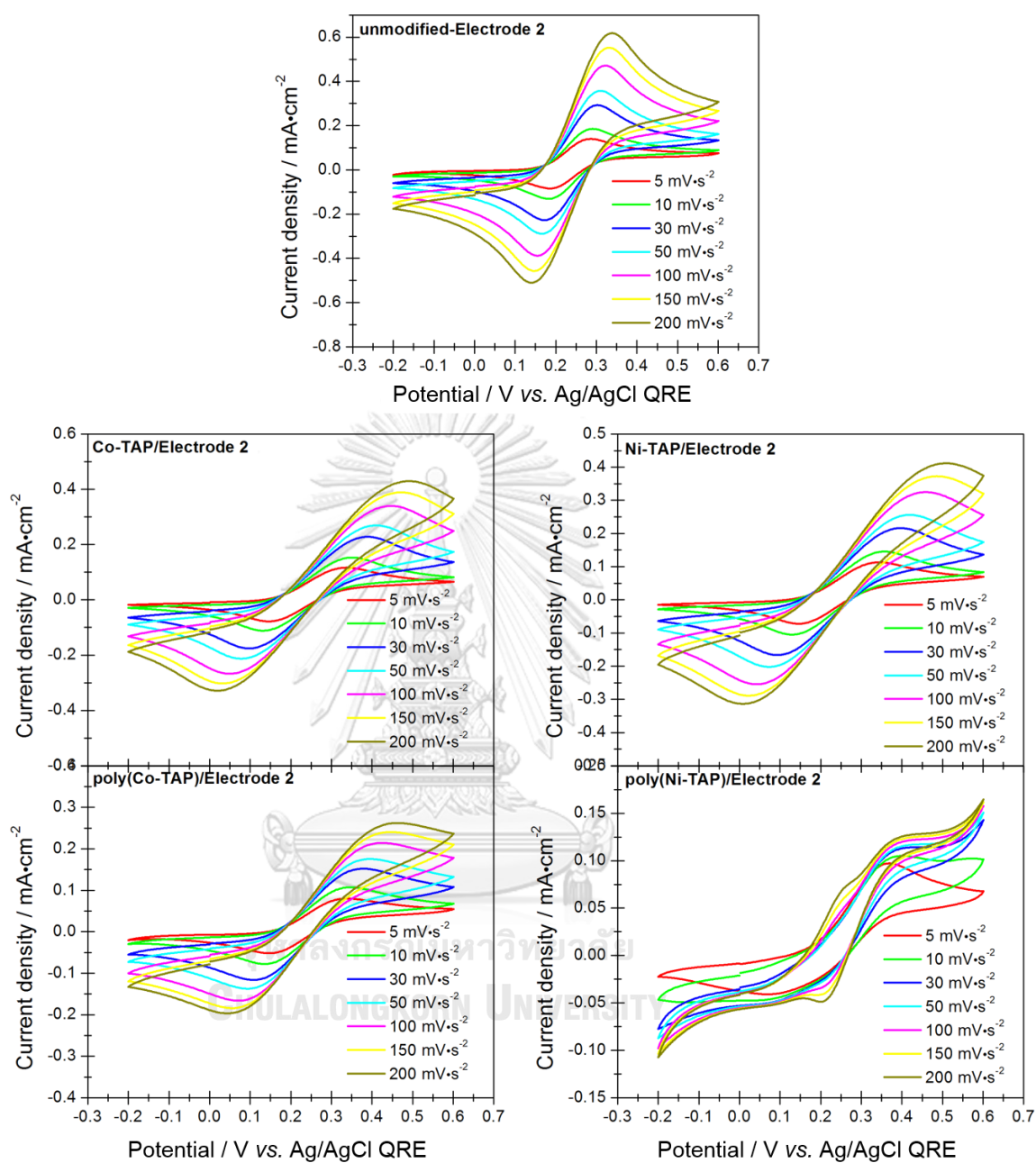


**Figure S7.** Cyclic voltammograms of phthalocyanine-modified and unmodified **Electrode 2** in 1.0 M a KCl aqueous solution containing 5.0 mM  $K_4Fe(CN)_6$  at scan rates of 5, 10, 30, 50, 100, 150 and 200  $mV \cdot s^{-1}$

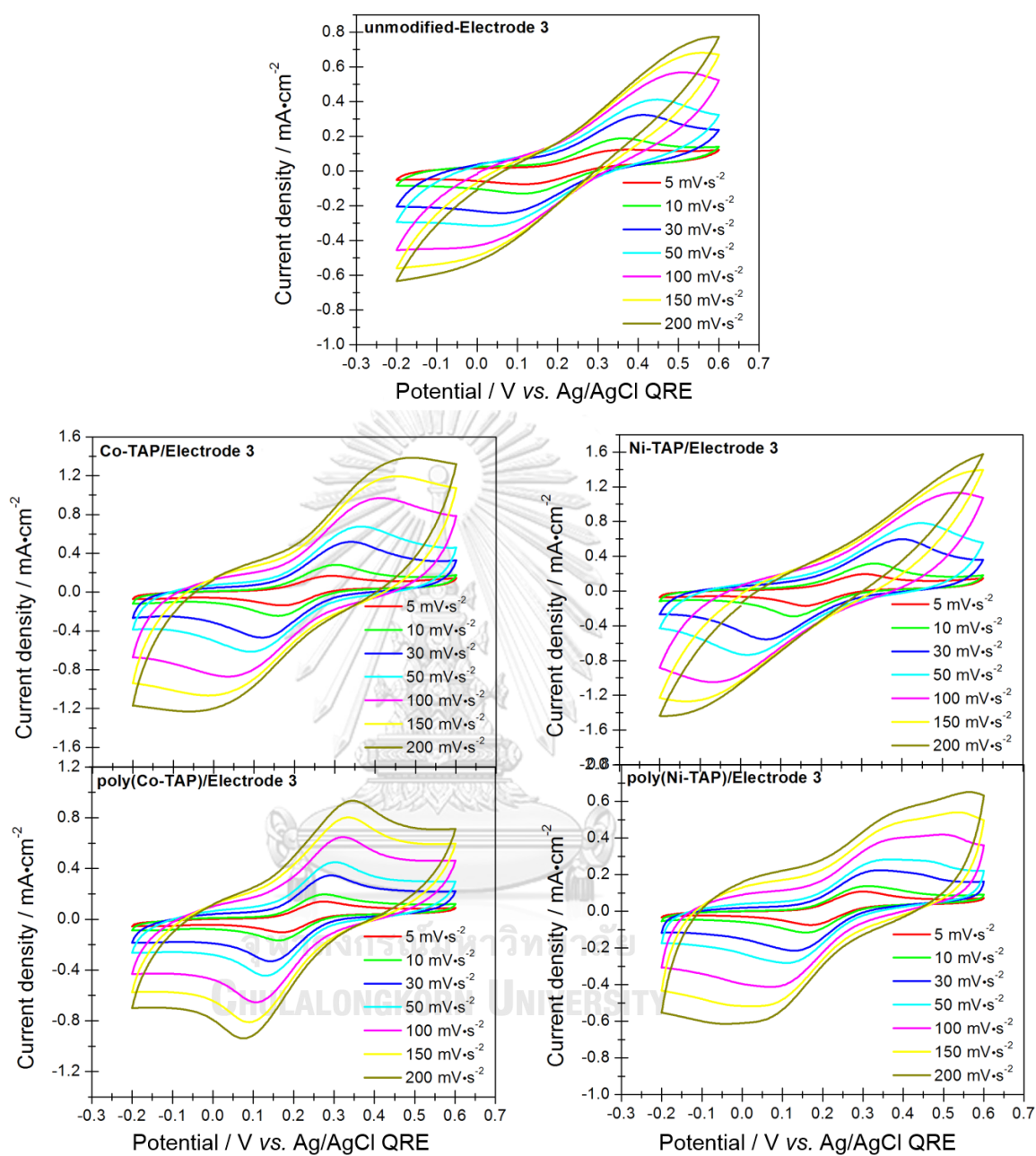
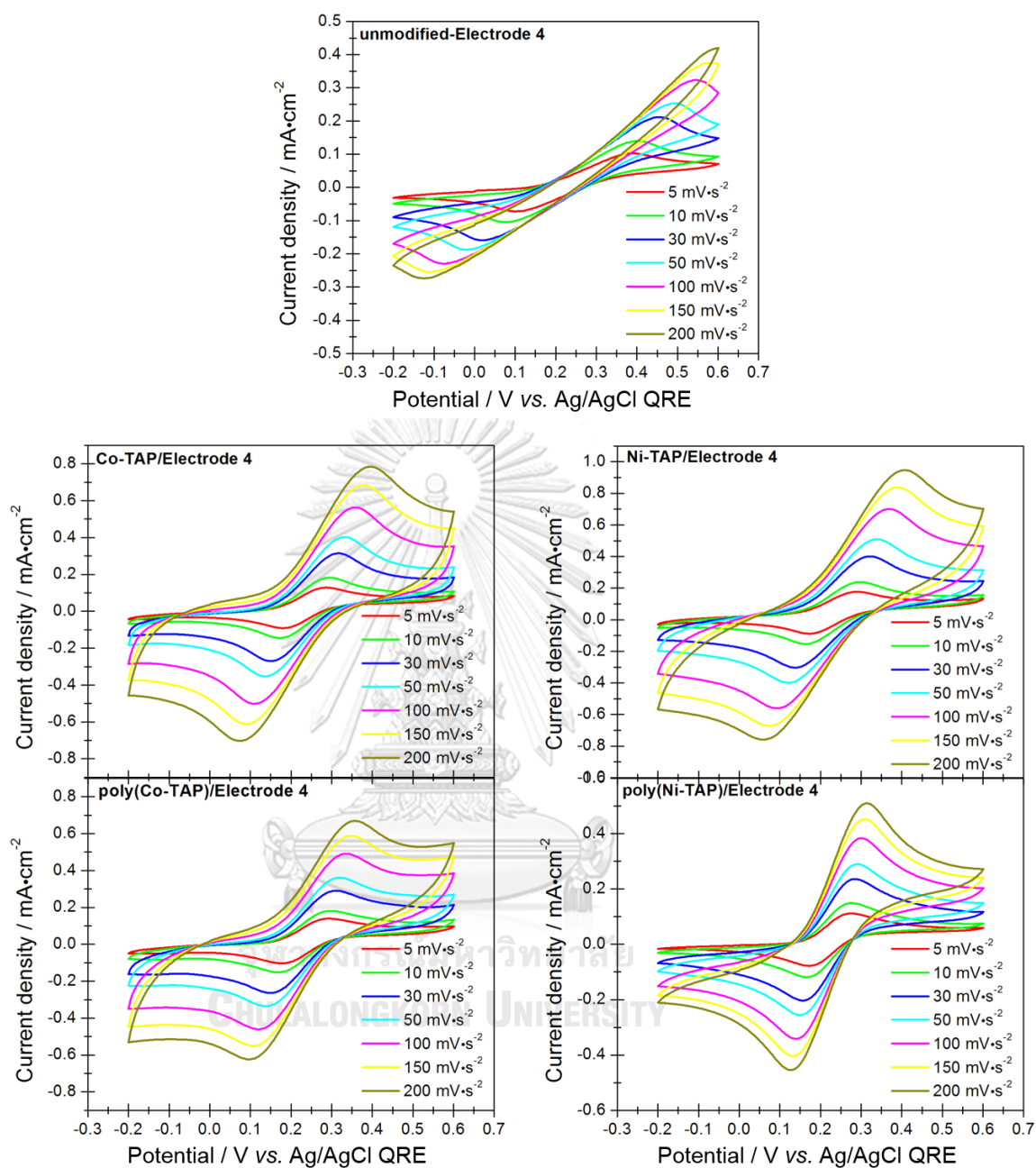


Figure S8. Cyclic voltammograms of phthalocyanine-modified and unmodified Electrode 3 in 1.0 M a KCl aqueous solution containing 5.0 mM  $K_4Fe(CN)_6$  at scan rates of 5, 10, 30, 50, 100, 150 and 200  $mV \cdot s^{-1}$





**Figure S9.** Cyclic voltammograms of phthalocyanine-modified and unmodified **Electrode 4** in 1.0 M a KCl aqueous solution containing 5.0 mM  $K_4Fe(CN)_6$  at scan rates of 5, 10, 30, 50, 100, 150 and 200  $mV \cdot s^{-1}$



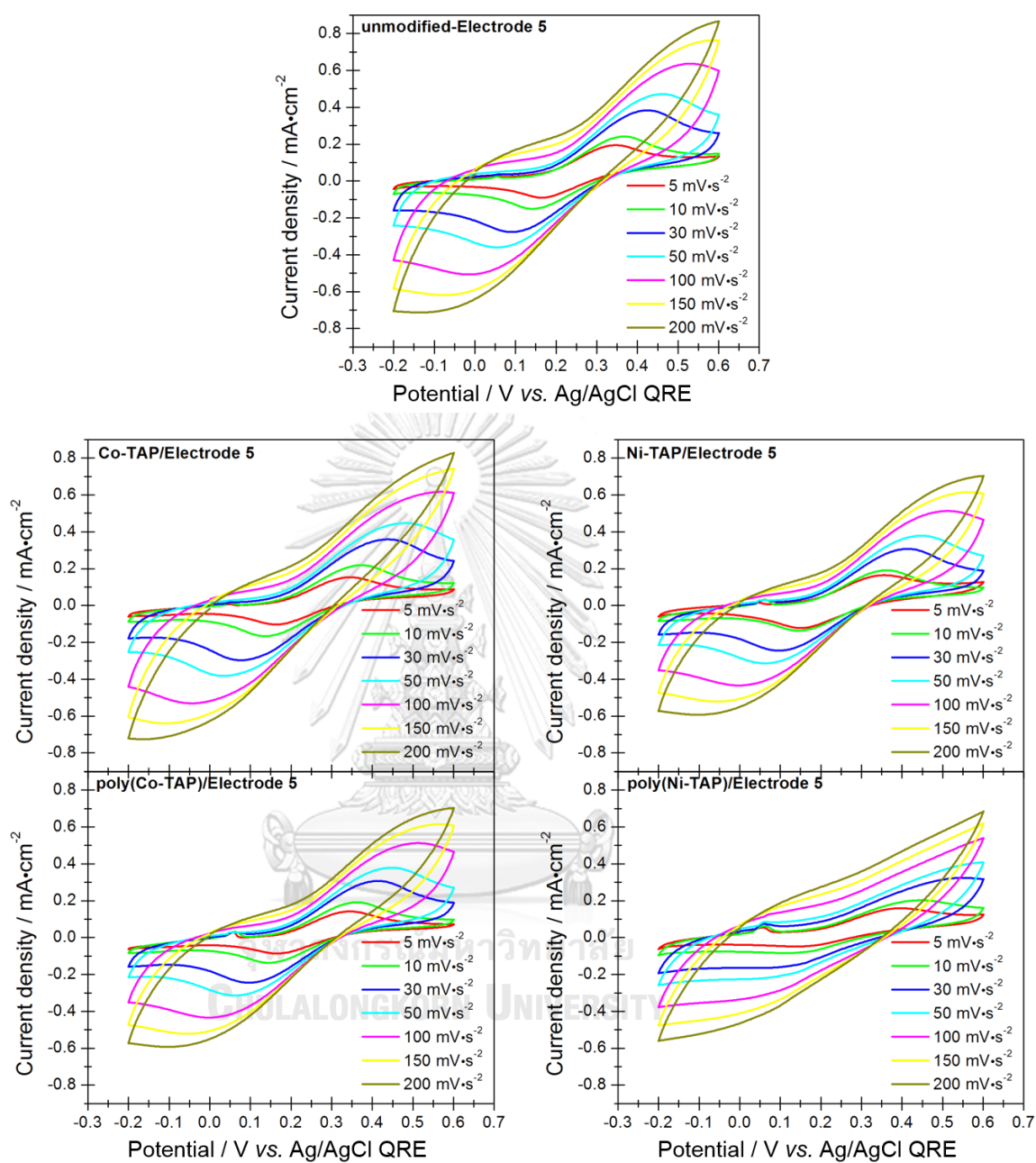


**Figure S10.** Cyclic voltammograms of phthalocyanine-modified and unmodified **Electrode 5** in 1.0 M a KCl aqueous solution containing 5.0 mM  $\text{K}_4\text{Fe}(\text{CN})_6$  at scan rates of 5, 10, 30, 50, 100, 150 and 200  $\text{mV}\cdot\text{s}^{-1}$

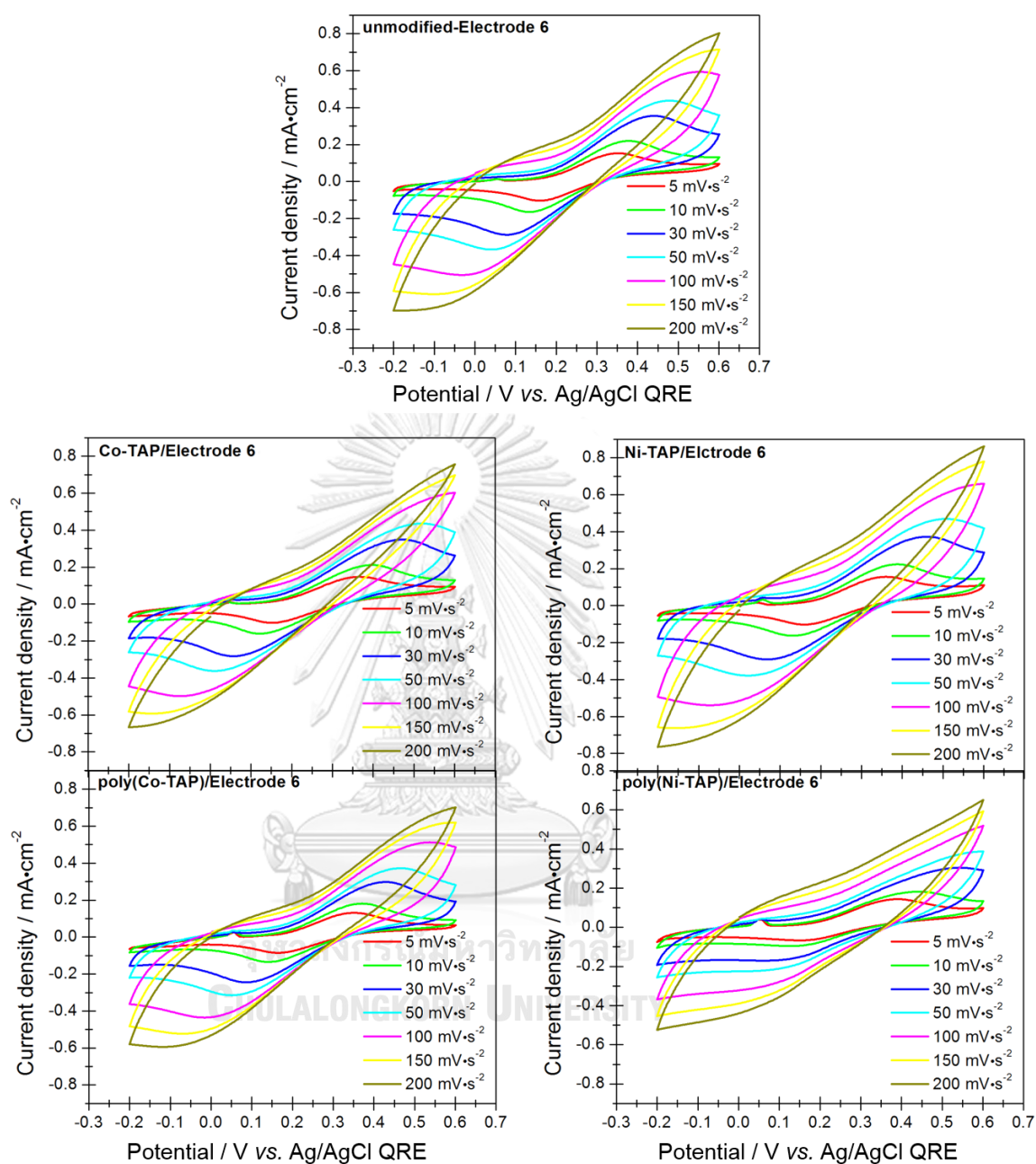


**Figure S11.** Cyclic voltammograms of phthalocyanine-modified and unmodified **Electrode 6** in 1.0 M a KCl aqueous solution containing 5.0 mM  $K_4Fe(CN)_6$  at scan rates of 5, 10, 30, 50, 100, 150 and 200  $mV \cdot s^{-1}$

## REFERENCES

1. Tarascon, J. M.; Armand, M. Issues and Challenges Facing Rechargeable Lithium Batteries. *Nature*, **2001**, *414*, 359–367.
2. Armand, M.; Tarascon, J. M. Building Better Batteries. *Nature*, **2008**, *451*, 652–657.
3. Philippe, P.; Franck, D. Clean Energy New Deal for a Sustainable World: from Non-CO<sub>2</sub> Generating Energy Sources to Greener Electrochemical Storage Devices. *Energy Environ. Sci.*, **2011**, *4*, 2003–2019.
4. S., T. B.; Bryony, T. M.; Peng-Fei, L.; Dwight, S. S. The Rise of Organic Electrode Materials for Energy Storage. *Chem. Soc. Rev.*, **2016**, *45*, 6345–6404.
5. Larcher, D.; Tarascon, J. M. Towards Greener and More Sustainable Batteries for Electrical Energy Storage. *Nat. Chem.*, **2014**, *7*, 19–29.
6. Carlos, A. M.; Xikang, F. On the Electrochemical Behavior of Iron Phthalocyanine Film Electrodes in Acid Solution. *J. Electrochem. Soc.*, **1983**, *130*, 811–814.
7. Armand, M. T., J. M. Researchers Must Find a Sustainable Way of Providing the Power our Modern Lifestyles Demand. *Nature*, **2008**, *451*, 652–657.
8. Bernstein, P. A.; Lever, A. B. P. Two-electron Oxidation of Cobalt Phthalocyanines by Thionyl Chloride Implications for Lithium/Thionyl Chloride Batteries. *Inorg. Chem.*, **1990**, *294*, 608–616.
9. Eunjoon, Y.; Haoshen, Z. Fe Phthalocyanine Supported by Graphene Nanosheet as Catalyst in Li-Air Battery with the Hybrid Electrolyte. *J. Power Sources*, **2013**, *244*, 429–434.
10. Priya, M. K.; Neena, S. J. Supercapacitor Application of Nickel Phthalocyanine Nanofibres and its Composite with Reduced Graphene Oxide. *Appl. Surf. Sci.*, **2018**, *449*, 528–539.
11. Jae-Hun, K.; Kai, Z.; Yanfa, Y.; Craig, L. P.; Arthur, J. F. Microstructure and Pseudocapacitive Properties of Electrodes Constructed of Oriented NiO-TiO<sub>2</sub> Nanotube Arrays. *Nano Lett.*, **2010**, *10*, 4099–4104.

12. Hui, X.; Michael, D. S.; Mahalingam, B.; Christopher, S. J.; Tijana, R. Amorphous TiO<sub>2</sub> Nanotube Anode for Rechargeable Sodium Ion Batteries. *J. Phys. Chem. Lett.*, **2011**, *2*, 2560–2565.
13. J., Z.; Zhao, X. S. Conducting Polymers Directly Coated on Reduced Graphene Oxide Sheets as High-Performance Supercapacitor Electrodes. *J. Phys. Chem. C.*, **2012**, *116*, 5420–5426.
14. Murugana, A. V.; Quintin, M.; Delville, M.-H.; Campet, G.; Gopinath, C. S.; Vijayamohan, K. Exfoliation- induced Nanoribbon Formation of poly( 3,4-ethylenedioxythiophene) PEDOT Between MoS<sub>2</sub> Layers as Cathode Material for Lithium Batteries. *J. Power Sources*, **2006**, *156*, 615–619.
15. Elgrishi, N.; Rountree, K. J.; McCarthy, B. D.; Rountree, E. S.; Eisenhart, T. T.; Dempsey, J. L. A Practical Beginner's Guide to Cyclic Voltammetry. *J. Chem. Educ.*, **2017**, *95*, 197–206.
16. Kissinger, P. T.; Heineman, W. R. Cyclic voltammetry. *J. Chem. Educ.*, **1983**, *60*, 702–706.
17. Andrade, C.; Oliveira, M. D.; Faulin, T.; Hering, V.; Abdalla, D. S. P. Biosensors for detection of Low-Density Lipoprotein and its modified forms, In *Biosensors for Health, Environment and Biosecurity*, IntechOpen: Rijeka. **2011**.
18. Liuyang, Z.; Hao, G. Improvement in Flexibility and Volumetric Performance for Supercapacitor Application and the Effect of Ni- Fe Ratio on Electrode Behaviour. *J. Mater. Chem. A.*, **2015**, *3*, 7607–7615.
19. Hsia, B. , Materials Synthesis and Characterization for Micro- supercapacitor Applications. PhD thesis, University of California, Berkeley, 2013, [http://digitalassets.lib.berkeley.edu/etd/ucb/text/Hsia\\_berkeley\\_0028E\\_13892.pdf](http://digitalassets.lib.berkeley.edu/etd/ucb/text/Hsia_berkeley_0028E_13892.pdf) (accessed October 10, 2019)
20. Bio- Logic Science Instruments, Electrochemistry Application, Protocols for studying intercalation electrodes materials : Part I: Galvanostatic cycling with potential limitation (GCPL). 2018. <https://www.bio-logic.net/wp-content/uploads/AN1.pdf> (accessed October 10, 2019).
21. MIT Electric Vehicle Team, A Guide to Understanding Battery Specifications, Battery Technical Specifications. 2008. (accessed October 10, 2019).

22. McKeown, N. B. Phthalocyanines. In *Comprehensive Coordination Chemistry II*, McCleverty, J. A.; Meyer, T. J., Eds. Pergamon: Oxford. **2003**.
23. Leznoff, C. C.; Lever, A. B. P. *Phthalocyanines: Properties and Applications*, VCH: New York. **1989**.
24. Zagal, J. H.; Bedioui, F.; Dodelet, J. P. *N4-macrocyclic Metal Complexes*, Springer, New York. **2006**.
25. Koodlur, S. L.; Karolien, D. W.; Annemie, A. Self-Assembled Supramolecular Array of Polymeric Phthalocyanine on Gold for the Determination of Hydrogen Peroxide. *Langmuir*, **2010**, *26*, 17665–17673.
26. Wolfgang, E.; Michael, H. Synthesis of Hexadecaalkoxy-Substituted Nickel and Iron Phthalocyanines. *Synthesis*, **1997**, *1*, 95–100.
27. Leznoff, C. C.; Marcuccio, S. M.; Greenberg, S.; Lever, A. B. P.; Tomer, K. B. Metallophthalocyanine Dimers Incorporating Five-atom Covalent Bridges. *Can. J. Chem.*, **1985**, *63*, 623–631.
28. Achar, B. N.; Lokesh, K. S. Studies on Tetra-amine Phthalocyanines. *J. Organomet. Chem.*, **2004**, *689*, 3357–3361.
29. Cosnier, S.; A., K. *Electropolymerization; Concepts, Materials and Applications*. Wiley-VCH, **2010**.
30. Li, H.; Guarr, T. F. Formation of Electronically Conductive Thin Films of Metal Phthalocyanines via Electropolymerization. *Chem. Commun.*, **1989**, *13*, 832–834.
31. Sivanesan, A.; Abraham, S. J. Amino Group Positions Dependent Morphology and Coverage of Electropolymerized Metallophthalocyanine (M = Ni and Co) Films on Electrode Surfaces. *Electrochim. Acta.*, **2008**, *53*, 6629–6635.
32. Bernstein, P. A.; Lever, A. B. P. Two-Electron Oxidation of Cobalt Phthalocyanines by Thionyl Chloride. Implications for Lithium/Thionyl Chloride Batteries. *Inorg. Chem.*, **1990**, *29*, 616–626.
33. Zhanwei, X.; Zhi, L.; Chris, M. B. H.; Xuehai, T.; Huanlei, W.; Babak, S. A.; Tyler, S.; David, M. Electrochemical Supercapacitor Electrodes from Sponge-like Graphene Nanoarchitectures with Ultrahigh Power Density. *J. Phys. Chem. Lett.*, **2012**, *3*, 2928–2933.
34. Yekang, W.; Jun, C.; Changcong, J.; Nengwen, D.; Chunxiang, W.; Dong, L.; Xiaolin, L.; Qian, Z.; Zhifeng, L.; Shengwen, Z. Tetra- $\beta$ -Nitro-Substituted Phthalocyanines:

- A New Organic Electrode Material for Lithium Batteries. *J. Solid State Electrochem.*, **2017**, *21*, 947–954.
35. Yoshihiko, K.; Kayano, S.; Tomokazu, I.; Kazuhito, H.; Akira, F. Photocatalytic Bactericidal Effect of TiO<sub>2</sub> Thin Films: Dynamic View of the Active Oxygen Species Responsible for the Effect. *J. Photoch. Photobio. A.*, **1997**, *106*, 51–56.
36. Moaaed, M.; Shaheer, M. A.; Nasser, A. M. B.; Hamza, A. M.; O-Bong, Y.; Hak-Yong, K. High-Efficiency Electrode Based on Nitrogen-Doped TiO<sub>2</sub> Nanofibers for Dye-Sensitized Solar Cells. *Electrochim. Acta*, **2014**, *115*, 493–498.
37. Adachi, M.; Yusuke, M.; Issei, O.; Susumu, Y. Formation of Titania Nanotubes and Applications for Dye-Sensitized Solar Cells. *J. Electrochem. Soc.*, **2003**, *150*, 488–493.
38. Ohsaki, Y.; Naruhiko, M.; Takayuki, K.; Yuji, W.; Takumi, O.; Toru, S.; Kohichi, N.; Shozo, Y. Dye-sensitized TiO<sub>2</sub> Nanotube Solar Cells: Fabrication and Electronic Characterization. *Phys. Chem. Chem. Phys.*, **2005**, *7*, 4157–4163.
39. Martti, K.; Candace, K. C.; Ma, J.; Yi, C.; George, G. Printable Thin Film Supercapacitors Using Single-Walled Carbon Nanotubes. *Nano. Lett.*, **2009**, *9*, 1872–1876.
40. Yong-Gang, W.; Zi-Dong, W.; Yong-Yao, X. An Asymmetric Supercapacitor Using RuO<sub>2</sub>/TiO<sub>2</sub> Nanotube Composite and Activated Carbon Electrodes. *Electrochim. Acta*, **2005**, *50*, 5641–5646.
41. Groenendaal, L. B.; Jonas, F.; Freitag, D.; Pielartzik, H.; Reynolds, J. R. Poly(3,4-Ethylenedioxythiophene) and Its Derivatives: Past, Present, and Future. *Adv. Mater.*, **2000**, *12*, 481–494.
42. Kirchmeyer, S.; Reuter, K. Scientific Importance, Properties and Growing Applications of Poly(3,4-Ethylenedioxythiophene). *J. Mater. Chem. A.*, **2005**, *15*, 2077–2088.
43. Jonas, F.; Schrader, L. Conductive Modifications of Polymers with Polypyrroles and Polythiophenes. *Synthetic Metals*, **1991**, *41*, 831–836.
44. Carlberg, J. C.; Inganas, O. Poly(3,4-ethylenedioxythiophene) as Electrode Material in Electrochemical Capacitors. *J. Electrochem. Soc.*, **1997**, *144*, 61–64.
45. Murugan, A. V.; Kale, B. B.; Kwon, C.-W.; Campet, G.; Vijayamohan, K. Synthesis and Characterization of a New Organo–Inorganic Poly(3,4-ethylenedioxythiophene) PEDOT/V<sub>2</sub>O<sub>5</sub> Nanocomposite by Intercalation. *J. Mater. Chem.*, **2001**, *11*, 2470–2475.

46. Chen, D.; Ji, G.; Ma, Y.; Lee, J.; Lu, J. Graphene-Encapsulated Hollow Fe<sub>3</sub>O<sub>4</sub> Nanoparticle Aggregates as a High-Performance Anode Material for Lithium Ion Batteries. *Appl. Mater. Interfaces*, **2011**, *3*, 3078–3083.
47. Park, S.; Ruoff, R. S. Chemical Methods for the Production of Graphenes. *Nat. Nanotechnol.*, **2009**, *4*, 217–224.
48. Bagri, A.; Mattevi, C.; Acik, M.; Chabal, Y. J.; Chhowalla, M.; Shenoy, V. B. Structural Evolution During the Reduction of Chemically Derived Graphene Oxide. *Nat. Chem.*, **2010**, *2*, 581–587.
49. Lim, Y. S.; Tan, Y. P.; Lim, H. N.; Huang, N. M.; Tan, W. T. Preparation and Characterization of Polypyrrole/ Graphene Nanocomposite Films and their Electrochemical Performance. *J. Polym. Res.*, **2013**, *20*, 156–165.
50. Laua, S. C.; Lima, H. N.; Ravoof, T. B. S. A.; Yaacob, M. H.; Grant, D. M.; MacKenzie, R. C. I.; Harrison, I.; M., H. N. A Three-Electrode Integrated Photo-Supercapacitor Utilizing Graphene- Based Intermediate Bifunctional Electrode. *Electrochim. Acta*, **2017**, *238*, 178-184.
51. Koodlur, S. L.; Annemie, A. Synthesis and Characterization of Tetra-substituted Palladium Phthalocyanine Complexes. *Dyes Pigm.*, **2013**, *96*, 269–277.
52. Mani, V.; Huang, S.; Devasenathipathy, R.; Yang, T. C. K. Electropolymerization of Cobalt Tetraaminophthalocyanine at Reduced Graphene Oxide for Electrochemical Determination of Cysteine and Hydrazine. *RSC Adv.*, **2016**, *6*, 38463–38469.
53. Zhong- Yong, Y.; Bao- Lian, S. Titanium Oxide Nanotubes, Nanofibers and Nanowires. *Colloid Surf. A Physicochem. Eng. Asp.*, **2004**, *241*, 173–183.
54. Yoshinori, O.; Naruhiko, M.; Takayuki, K.; Yuji, W.; Takumi, O.; Toru, S.; Kohichi, N.; Shozo, Y. Dye-sensitized TiO<sub>2</sub> Nanotube Solar Cells: Fabrication and Electronic Characterization. *Phys. Chem. Chem. Phys.*, **2005**, *7*, 4157–4163.
55. Nacer, S.; Salah, A.; Jean-Jacques, A.; Mohamed, J.; Jean, C. L.; Pierre-Camille, L. Improvement of the Electrosynthesis and Physicochemical Properties of Poly(3,4-ethylenedioxythiophene) Using a Sodium Dodecyl Sulfate Micellar Aqueous Medium. *Langmuir*, **1999**, *15*, 2566–2574.

56. Lim, Y. S.; Tan, Y. P.; Lim, H. N.; Huang, N. M.; Tan, W. T. Preparation and Characterization of Polypyrrole/ graphene Nanocomposite Films and their Electrochemical Performance. *J. Polym. Res*, **2013**, *20*, 156–165.
57. Alejandro, G.-M. F.; Christopher, W. F.; Peter, J. K.; B., D. A. C.; B., C. E. Determination of the Electrochemical Area of Screen-Printed Electrochemical Sensing Platforms. *Biosensors*, **2018**, *8*, 53–62.
58. EL-CELL electrochemical test equipment. User Manual: ECC-Ref Electrochemical test cell with reference electrode. [https://el-cell.com/wp-content/uploads/downloads/manuals/Manual\\_ECC-Ref\\_Release\\_2.5.pdf](https://el-cell.com/wp-content/uploads/downloads/manuals/Manual_ECC-Ref_Release_2.5.pdf) (accessed Oct 25, 2019).
59. Mashazi, P.; Togo, C.; Limson, J.; Nyokong, T. Applications of Polymerized Metal Tetra- amino Phthalocyanines Towards Hydrogen Peroxide Detection. *J. Porphyr. Phthalocya.*, **2010**, *14*, 252–263.
60. Copper Phthalocyanines: Paint and Coating Industry <https://www.pcimag.com/articles/83452-copper-phthalocyanines> (accessed Aug 28,2019).
61. Sivamalar, S.; Shanthi, J.; Kalugasalam, P. Comparison of Optical Properties of PbPc and CuPc Thin Films. *Chalcogenide Lett.*, **2012**, *9*, 287–297.
62. Achar, B.; Lokesh, K. Studies on Tetra-amine Phthalocyanines. *J. Organomet. Chem.*, **2004**, *689*, 3357–3361.
63. Jeevagan, A. J.; John, S. A. Synthesis of Non-Peripheral Amine Substituted Nickel(II) Phthalocyanine Capped Gold Nanoparticles and their Immobilization on Electrode for the Electrocatalytic Oxidation of Hydrazine. *RSC Adv.*, **2013**, *3*, 2256–2264.
64. Alonso, R. M.; San-Martin, M. I.; Sotres, A.; Escapa, A. Graphene Oxide Electrodeposited Electrode Enhances Start- Up and Selective Enrichment of Exoelectrogens in Bioelectrochemical Systems. *Sci. Rep.*, **2017**, *7*, 13726–13735.
65. Chien-Cheng, T.; Hsisheng, T. Structural Features of Nanotubes Synthesized from NaOH Treatment on TiO<sub>2</sub> with Different Post-Treatments. *Chem. Mater.*, **2006**, *18*, 367–373.
66. Manrico, F.; Kamil, Z.; Colin, H.; Peter, M.; Hans, J. G. The Role of Water in the Synthesis and Performance of Vapour Phase Polymerised PEDOT Electrochromic Devices. *J. Mater. Chem.*, **2009**, *19*, 7871–7878.



67. Jiao, W.; Kefeng, C.; Shirley, S. A Facile Chemical Reduction Approach for Effectively Tuning Thermoelectric Properties of PEDOT films. *Org. Electron.*, **2015**, *17*, 151–158.
68. Fan, L. Q.; Liu, G. J.; Wu, J. H.; Liu, L.; Lin, J. M.; Wei, Y. L. Asymmetric Supercapacitor Based on Graphene Oxide/Polypyrrole Composite and Activated Carbon Electrodes. *Electrochim. Acta.*, **2014**, *137*, 26–33.
69. Rourke, F.; Crayston, A. J. Cyclic Voltammetry and Morphology of Polyaniline-coated Electrodes containing  $[\text{Fe}(\text{CN})]^{3-/4-}$  Ions. *J. Chem. Soc. Faraday Trans.*, **1993**, *89*, 295–302.
70. Bolade, O. A.; Kenneth, I. O.; Tebello, N. Electrochemical Properties of Benzylmercapto and Dodecylmercapto Tetra Substituted Nickel Phthalocyanine Complexes: Electrocatalytic Oxidation of Nitrite. *Electrochim. Acta.*, **2006**, *51*, 6470–6478.
71. Kang, T. F.; Shen, G. L.; Yu, R. Q. Voltammetric Behaviour of Dopamine at Nickel Phthalocyanine Polymer Modified Electrodes and Analytical Applications. *Anal. Chim. Acta*, **1997**, *356*, 245–251.
72. Zahraa, A. J.; Mohammed, R. S.; Sulaiman, A. G. Conductive Polymers: Their Preparations and Catalyses on NADH Oxidation at Carbon Cloth Electrodes. *Arab. J. Chem.*, **2015**, *8*, 726–731.
73. Chun, L.; Toyoko, I. Electrochemical and Optical Properties of the Poly(3,4-ethylene-dioxythiophene) Film Electropolymerized in an Aqueous Sodium Dodecyl Sulfate and Lithium Tetrafluoroborate Medium. *Macromolecules*, **2004**, *37*, 2411–2416.
74. Sanjoy, M.; Utpal, R.; Sudip, M. Graphene Quantum Dot-Doped Polyaniline Nanofiber as High Performance Supercapacitor Electrode Materials. *Chem. Commun.*, **2015**, *51*, 12365–12368.



จุฬาลงกรณ์มหาวิทยาลัย  
**CHULALONGKORN UNIVERSITY**

## VITA

**NAME** Apinut Chongphanitkul

**DATE OF BIRTH** 8 September 1995

**PLACE OF BIRTH** Bangkok

**INSTITUTIONS ATTENDED** Bachelor of Science, Chemistry, Chulalongkorn University

**HOME ADDRESS** 212/224 Soi Petkrasaem 16 Petkrasaem Road  
Wat Tha Pra Bangkok Yai Bangkok 10600

